LA-UR-13-22561

Approved for public release; distribution is unlimited.

Title: Review of Data from Shock Physics Experiments SPE-1, SPE-2 and SPE-3: Data Corrections and Phenomenology Analysis

Author(s): Steedman, David W.

Intended for: Report

Issued: 2013-04-19 (Rev.3)

LA-UR-13-22561

Approved for public release; distribution is unlimited.

Title:	Review of Data from Shock Physics Experiments SPE-1, SPE-2 and SPE-3: Data Corrections and Phenomenology Analysis
Author(s):	Steedman, David W.
Intended for:	Report
Issued:	2013-04-18 (Rev.2) (Draft)

Review of Data from Shock Physics Experiments SPE-1, SPE-2 and SPE-3: Data Corrections and Phenomenology Analysis

David Steedman, Los Alamos National Laboratory

ACKNOWLEDGEMENT

The Source Physics Experiments (SPE) would not have been possible without the support of many people from several organizations. The author (s) wish to express their gratitude to the SPE working group, a multi-institutional and interdisciplinary group of scientists and engineers from National Security Technologies (NSTec), Lawrence Livermore National Laboratory (LLNL), Los Alamos National Laboratory (LANL), Sandia National Laboratories (SNL), the Defense Threat Reduction Agency (DTRA), and the Air Force Technical Applications Center (AFTAC). Deepest appreciation to Mssrs. Bob White and Ryan Emmitt (NSTec) for their tireless support on the seismic array and to the University of Nevada, Reno (UNR) for their support with the seismic network and data aggregation. Thanks to U.S. Geological Survey (USGS), the Incorporated Research Institutions for Seismology (IRIS) Program for Array Seismic Studies of the Continental Lithosphere (PASSCAL) Instrument Center, Lawrence Berkeley National Laboratory (LBNL), and Dr. Roger Waxler (University of Mississippi) for instrumentation partnership. The author(s) also wish to thank the National Nuclear Security Administration (NNSA), Defense Nuclear Nonproliferation Research and Development (DNN R&D) for their sponsorship of the National Center for Nuclear Security (NCNS) and its Source Physics Experiment (SPE) working group. This work was sponsored by the NNSA under award number DE-AC52-06NA25946.

INTRODUCTION

The NNSA is conducting a series of high explosive (HE) tests – the Source Physics Experiments – at the National Nuclear Security Site (NNSS). These experiments are intended to investigate the generation of geophysical signals from controlled sources. These signals will aid in the development of physics-based models to aid in the discrimination of signals emitted from these and other possible sources, such as earthquakes and clandestine nuclear events.

The SPE events include an array of accelerometers near to the source intended to provide measurements of the strong ground motion, or "near field," regime. LANL performed an extensive review of the near field measurements from the first two events (SPE-1 and SPE-2) in this series. This review revealed that the near field gauges likely rotated during installation, causing measurement uncertainty.

This conclusion led to the installation of new gauges for the third experiment, SPE-3, utilizing new physical design and improved installation practices to achieve better quality control on their orientation. A subsequent analysis of SPE-3 data confirmed that rotations occurred and provided the basis for corrections to those data where the amount of rotation could be credibly determined.

The corrected data supports a more confident analysis of the entire near field data set. This report summarizes the data errors and provides results of the analysis of the corrected dataset.

GAUGE CANISTER ROTATIONS

SPE-1 and SPE-2 Test Set-up

The SPE-1 and SPE-2 sources were right circular cylinders of sensitized heavy ammonium nitrate and fuel oil (SHANFO) explosive. SPE-1 was 100 kg and was fired at a depth of 180 ft in a borehole (U15n) drilled for this purpose. This was followed by the 1000-kg SPE-2 fired in the same 3-ft borehole at 150 ft. SPE-1 was conducted on 3 May 2011. SPE-2 was conducted on 25 October 2011. Figure 1 illustrates the test bed for these two events.

The experiments included an array of near field accelerometers to diagnose the close-in region. Specifically, there were six instrumentation holes on two concentric, 10-m and 20-m radius, rings around the charge hole. Holes 1, 2, and 3 were on a nominally 10-m radius circle while holes 4, 5, and 6 were on a nominally 20-m radius circle. (Official nomenclature for these holes includes the designation U15n and the hole number – *e.g.*, U15n#1 – but this report eliminates the "U15n#" portion of the names for clarity of reading.) Each hole included three 3-component accelerometer gauge packages at various depths. For each hole, gauge package 1 was at the SPE-1 shot depth (*i.e.*, 180 ft), gauge package 2 was at the SPE-2 shot depth (*i.e.*, 150 ft), and gauge package 3 was at the 50-ft depth. Each package included a transducer labeled "radial," one labeled "transverse," and a third labeled "longitudinal." Gauge packages are referred to by their respective hole and depth; *e.g.*, package 2-1 is in hole 2 at depth 1. Further, each individual transducer in the package is labeled by the first letter of its component; *e.g.*, measurement 2-1-R is the radial measurement in package 2-1.

However, due to the geometry of the test bed these components need further definition. The gauge packages at depths 1 and 2 are placed in a cylindrical coordinate system about the charge hole axis. In this design, the "radial" gauge, which strictly speaking is horizontal outward, is only truly radial for the charge placed at that depth. That is, gauge 2-1-R is a true radial for SPE-1, but is a horizontal component of the spherically propagating shock in SPE-2. Similarly, the longitudinal component is vertical, and 2-1-L is a true longitudinal (or vertically oriented tangential) measurement for SPE-1, but is a vertical component of the spherically propagating shock in SPE-2. The tangential measurement is a horizontal component normal to the R-T plane.

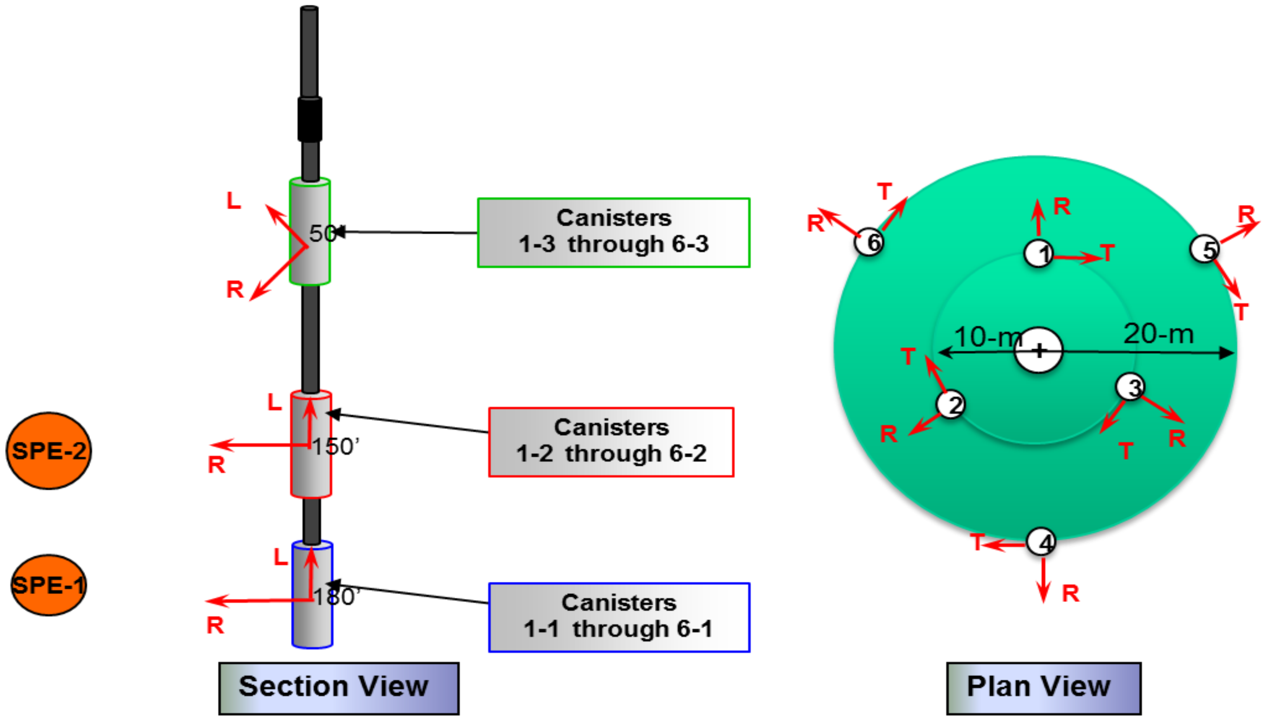

Figure 1: SPE-1/SPE-2 test layout.

The gauge packages at depth 3 are oriented in a spherical coordinate system with the origin at the SPE-2 shot point. So the radial gauge is truly radial for SPE-2 and approximately radial for the deeper SPE-1. Similarly, the longitudinal and transverse gauges are orthogonal tangential measurements on a sphere centered at SPE-2.

Note that several transducers in hole 1 failed during or after the SPE-1 event and a new hole (1A, not shown) was drilled near hole 1 (to the left of hole 1 on Figure 1) with an identical set of gauge canisters.

SPE-1 and SPE-2 Data

In these experiments the ground shock environment is expected to follow general well-established theory for geometric propagation of shock waves from a cylindrical, or near-spherical, source. Figure 2 provides an example of a set of velocity histories that conform to expectation at the shot depth for SPE-1. Gauge package 6-1 at the 20-m range is dominated by a large outward radial velocity normal to the shock with minor motion in the directions tangential (transverse and longitudinal) to the front.

But a review of other measurements in the SPE-1 set revealed some history sets that are not as consistent with expectations. For example, while another gauge package at the same depth and range (*i.e.*, 4-1, Figure 3) shows similarly weak transverse and longitudinal components, the large radial motion is *inward*, or opposite of what one would expect from a compressive, explosively driven shock.

However, the trend seen in gauge package 2-1 (Figure 4) at the 10-m range at the shot depth is problematic. The radial and transverse components are similar in amplitude for this location. That is, the transverse amplitude is exceedingly high in comparison to its co-located radial component. A prior report (Ref. 1) attributes this phenomenon to effects caused by local geologic anomalies on the shock field. Specifically, the hypothesis is that the joints sets cause “turning” of the shock due to excessive shear components. But no computational or physical evidence is provided to support the notion that this phenomenon can have this strong of an effect.

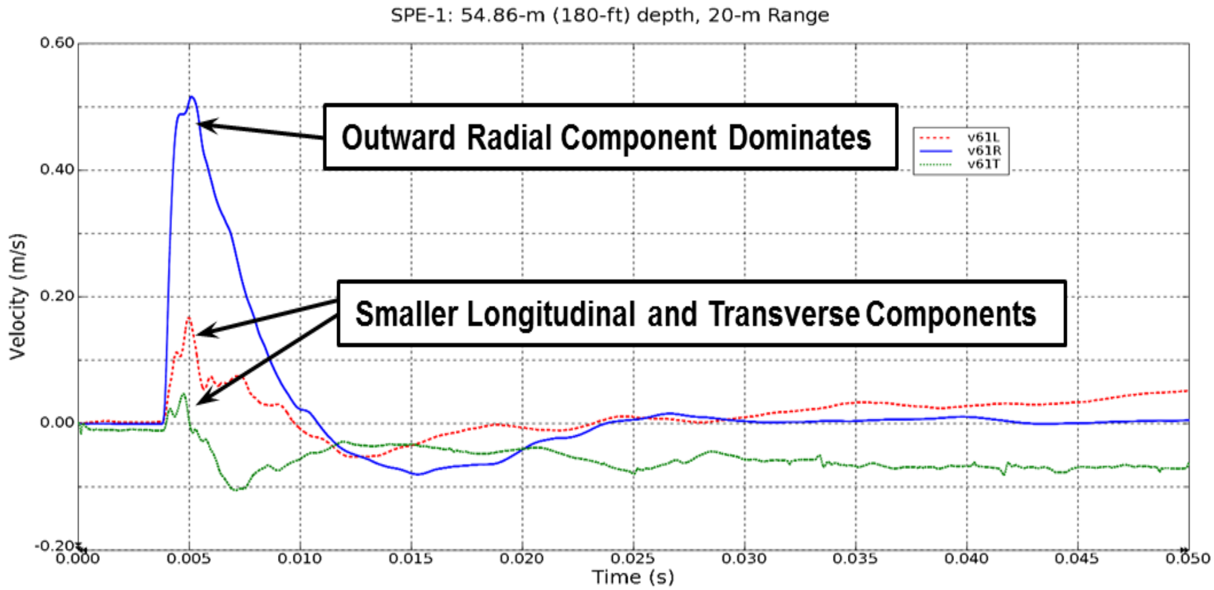

Figure 2: Consistent set of velocity histories for a cylindrical charge: gauge package 6-1.

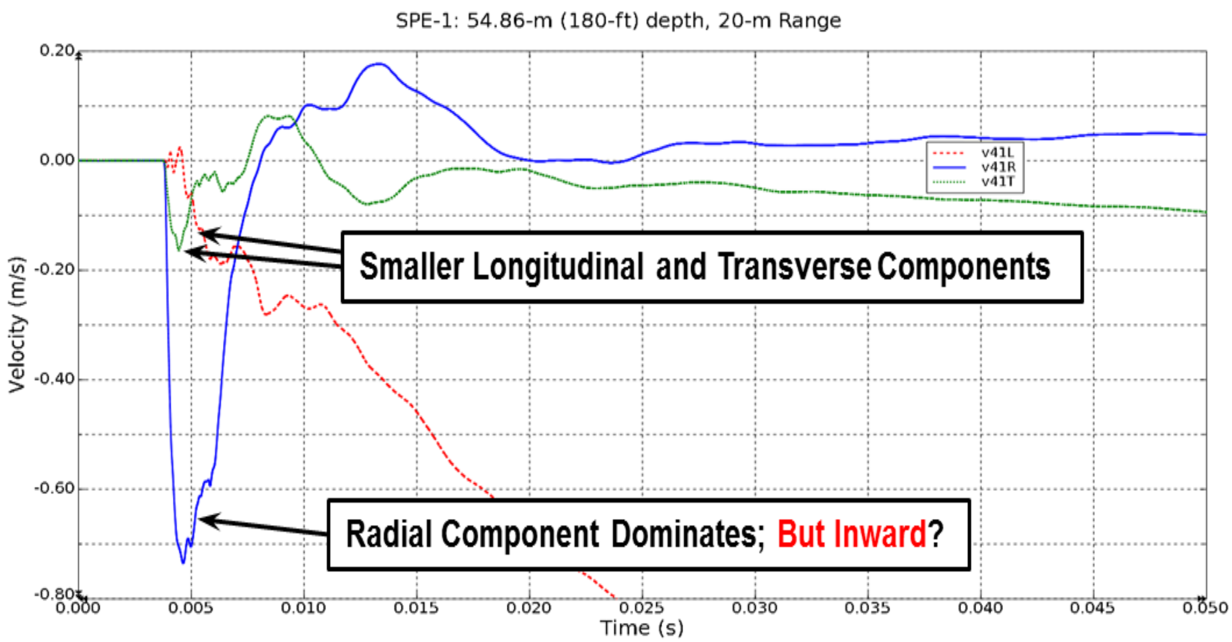

Figure 3: Consistent set of velocity histories for a cylindrical charge except for reversed direction radial: gauge package 4-1.

The data from gauge package 3-1 (Figure 5) at the 10-m range at the shot depth is more suspect. The radial measurement in this plot is suspiciously low in magnitude and does not have the characteristic strong outward phase one would expect. On the other hand, the transverse component possesses a strong pulse which, notwithstanding the algebraic sign, possesses the character expected of a radial measurement. This difference cannot be explained by local joint phenomenology.

Figure 4 and Figure 5 were used to illustrate relative response among the components in a given gauge package. Comparisons between data from different gauge packages also provide insight into problems with the gauges. Figure 6 includes one component from each of the gauges at the 10-m range at the shot depth in SPE-1. These are the radial measurement of 1-1 and the transverse components for 2-1 and 3-1 (note that 3-1 transverse is reversed in sign). The similarity in both magnitude and character for the measurements is significant considering the expected differences described in Figure 2. A similar observation is made in Figure 7 which includes the radial component for 2-1 which is nearly identical to the transverse measurement from 1-1. The fact that some transverse components closely track other radial components is compelling evidence of gauge rotation.

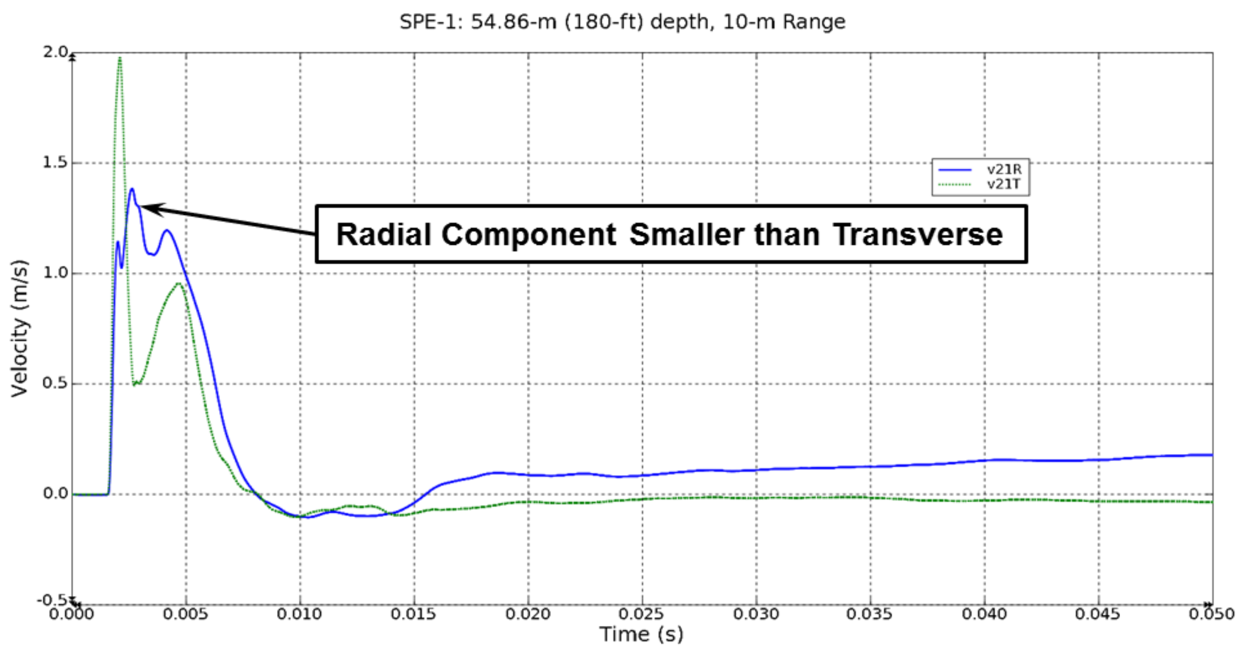

Figure 4: Inconsistent set of velocity histories for a cylindrical charge, including unexpectedly high transverse pulse relative the radial motion: gauge package 2-1.

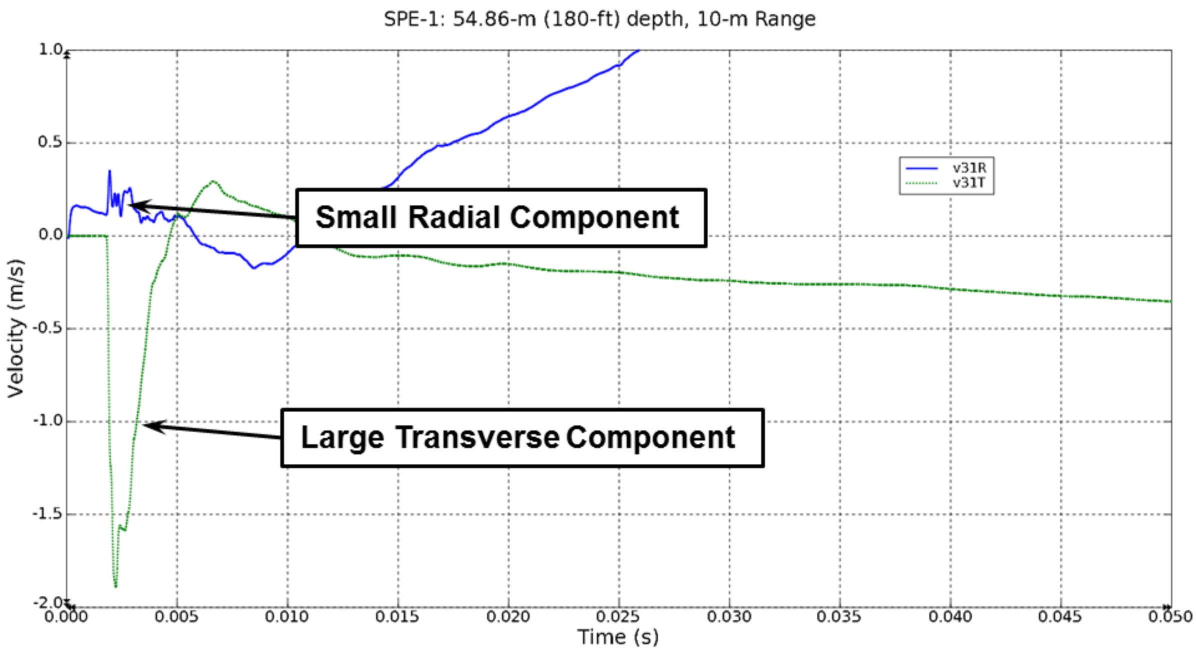

Figure 5: Inconsistent set of velocity histories for a cylindrical charge, including large transverse pulse with limited radial motion: gauge package 3-1.

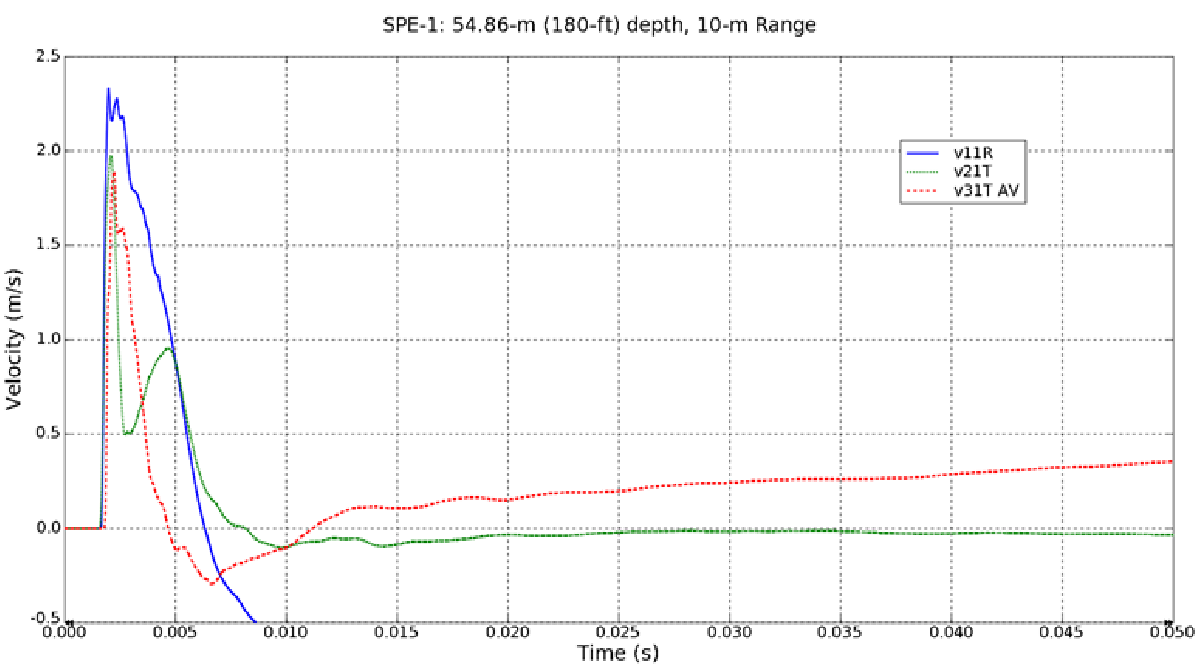

Figure 6: A radial velocity history (1-1) compared to two transverse velocity histories (2-1 and 3-1) at the same range and depth.

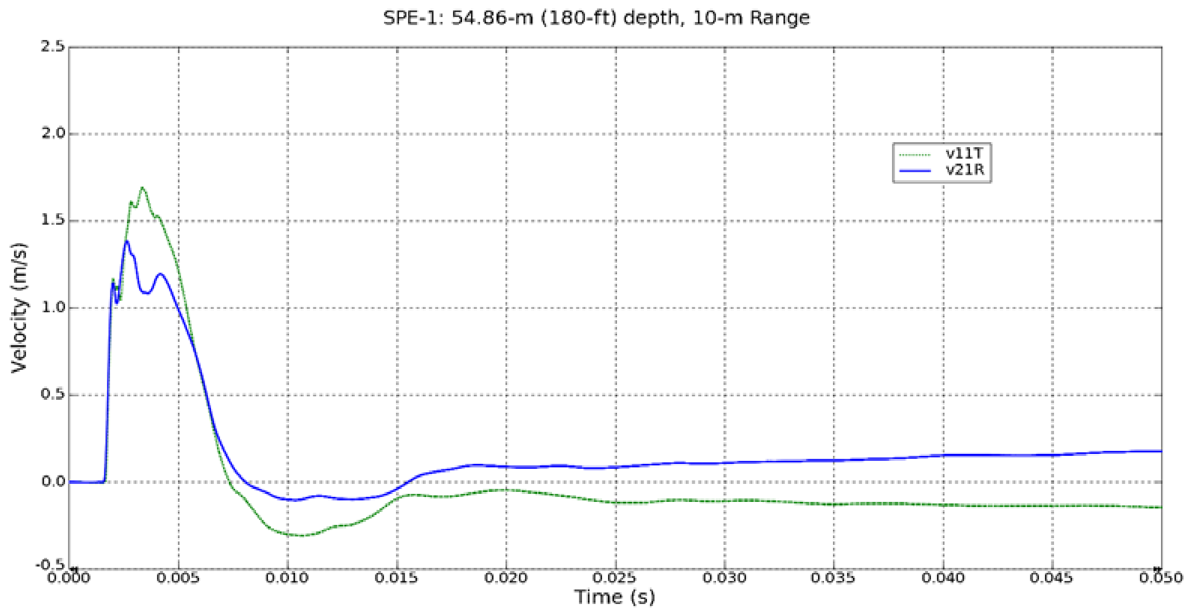

Figure 7: A radial velocity history (2-1) compared to a transverse velocity history (1-1) at the same range and depth.

Similar data anomalies are evident throughout the SPE-1 data set. Moreover, the anomalies were consistently repeated in SPE-2. Reference 2 and Reference 3 provide a comprehensive review of all data from these two events which will not be repeated here. Instead, the anomalies of the full data set can be summarized in data quality "stop light" charts (Figure 8). In this figure, green represents gauge packages where no apparent anomalies were observed and red represents gauge packages for which the recorded components suggest canister rotation. Black represents those locations for which no data were recovered due to inoperable gauges.

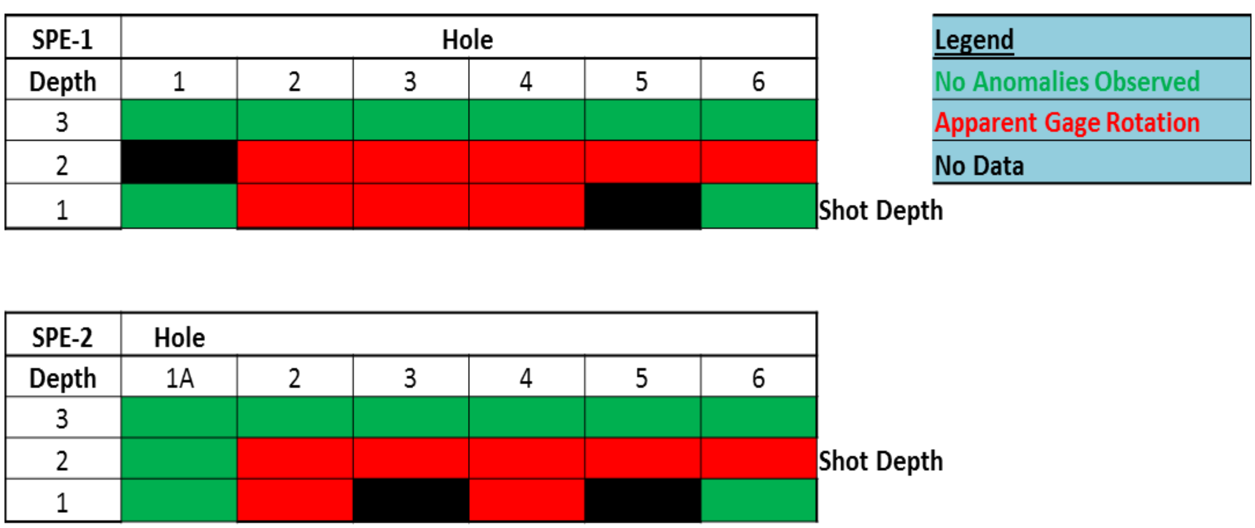

Figure 8: Stop light chart summarizing data anomalies for SPE-1 and SPE-2.

The two charts – one for each event – are consistent between the two events indicating persistence in anomalous behavior. Another pattern evident is that all gauge canisters at the 50-ft depth for both experiments performed as expected. These canisters are nearest to the surface and, thus, would have less opportunity to rotate. Finally, all canisters in hole 1A, described earlier as replacements for the failed hole 1 gauges, appeared to yield acceptable data. These replacement gauges were placed with better quality control than the older canisters (Ref. 5).

SPE-3 Test Set-up

The results presented above prompted the test team to include extra gauge canisters for SPE-3. These new canisters served two purposes: to provide redundant data for questionable canisters and to fill-in for areas of the test bed where more data coverage was desired. Figure 11 illustrates the layout of these new holes, numbered 7, 8, 9, 10, and 11.

Holes 7 and 8 on the 20-m and 10-m rings, respectively, and hole 11, 45 m from the charge hole, had canister depths identical to the older holes; that is, at 50 ft, 150 ft, and 180 ft from the ground surface. Hole 9 on the 20-m ring had canisters at those depths as well as at 90 ft and 120 ft from the ground surface. Hole 10 was a slant hole drilled from the surface location indicated through the SPE-2/SPE-3 charge center, and had a single radial (*i.e.*, in the line of the hole axis) transducer at a distance of 12 m from the charge.

SPE-3, conducted on 24 July 2012, was designed to be a repeat of SPE-2; *i.e.*, a charge in the same size container emplaced at the same location as SPE-2. But a change in final explosive density resulted in 900 kg in yield in the pre-fabricated canister. This difference in charge mass is inconsequential to the following discussion, and comparisons between the data from these two events provide adequate evidence into whether some canisters in holes 1 through 6 rotated during placement.

SPE-3 Data

Figure 10 presents the data for the radial and transverse transducers from canister 6-1 for shots SPE-2 and SPE-3. There were no data from the longitudinal transducers. This canister provides reasonable data in that a large outward radial measurement is accompanied by a relatively small transverse component. The records for both components are consistent between the two events.
Figure 11 presents the data for these same tests from canister 2-1 where the relative magnitudes between radial and transverse components were previously described to be questionable (Figure 4). As in SPE-1, the transverse component is larger than the radial component which is inconsistent with the response expected. The significant longitudinal component is a reasonable response as the canister is located 45^{o} below the shot point and so the radially propagating shock will have a significant vertical component. Similar to canister 6-1 all of the records for canister 2-1 are consistent between the two events.

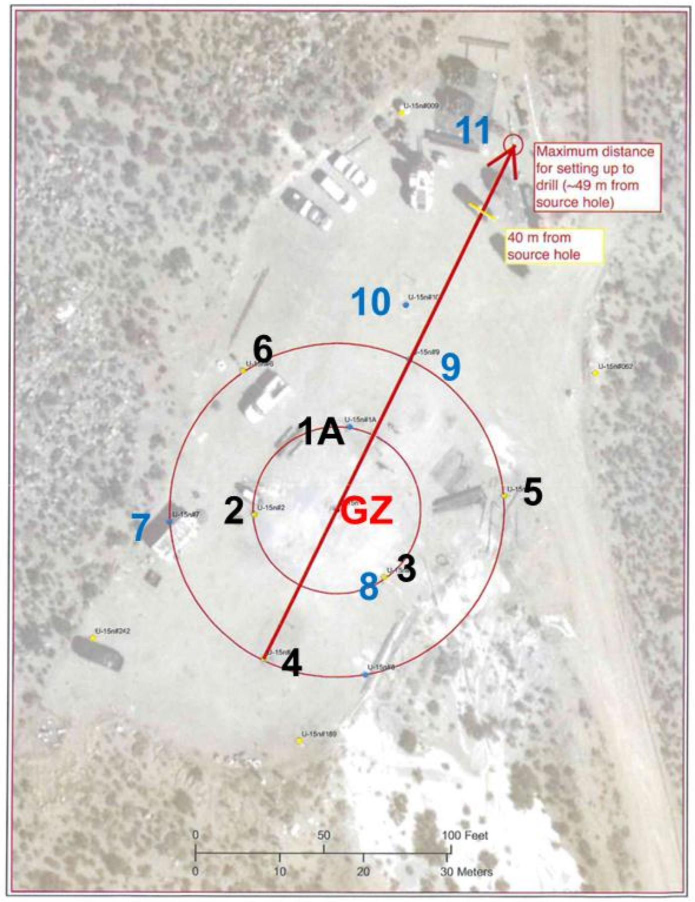

Figure 9: Instrument hole layout for SPE-3.

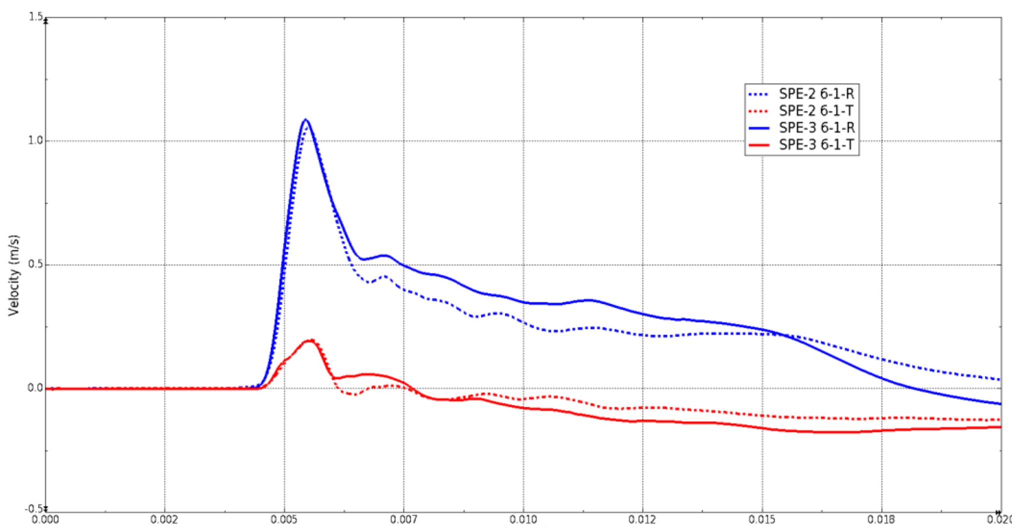

Figure 10: All data components recorded by canister 6-1 from both SPE-2 and SPE-3.

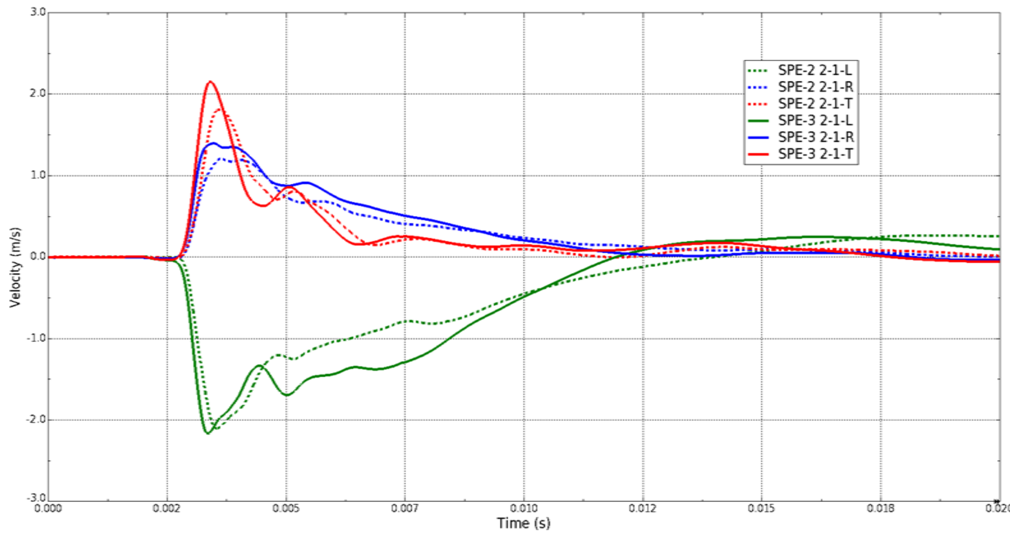

Figure 11: All data components recorded by canister 2-1 from both SPE-2 and SPE-3.

Figure 12 includes SPE-2 and SPE-3 data for canister 6-2 which was dominated completely by the supposed transverse measurement with apparently inconsequential motion in the radial direction. As with the prior examples, the histories for all transducers are very similar between the events. But there are notable differences between these two events for this canister at shot level. Specifically, the SPE-3 records have lower amplitude and later arrival times than the SPE-2 records. These differences will be discussed later.

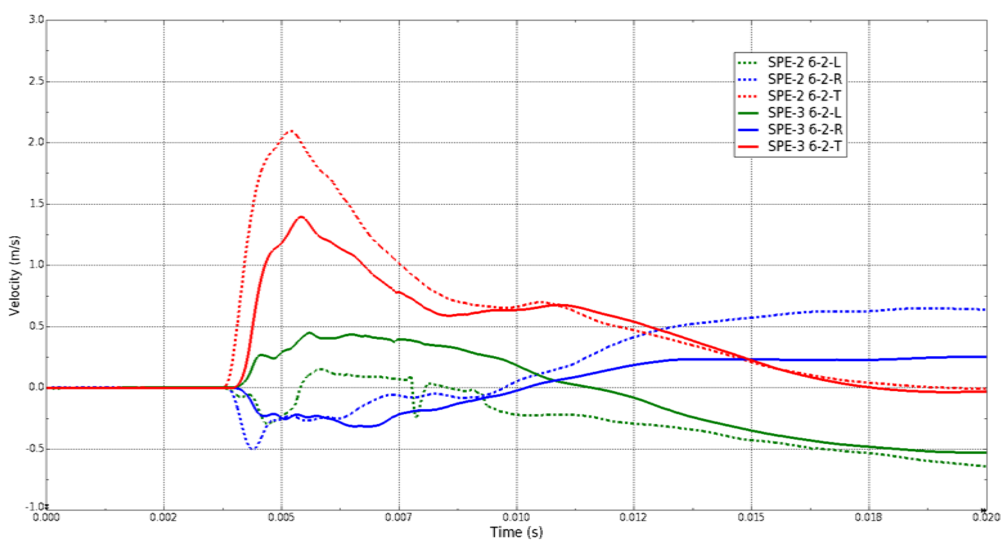

Figure 12: Velocity histories from location 6-2 for SPE-2 and SPE-3.

In the above examples, data from three canisters displayed consistency between two events with identical locations and nearly identical yields. It is an important observation that one of these (6-1) had reasonable radial-to-transverse component amplitude comparisons while the other two (2-1 and 6-2) provided unexpectedly high transverse magnitudes relative to their respective radial magnitudes. This provides evidence that SPE-3 was a reasonable replication of SPE-2, thus allowing comparisons between SPE-3 histories from questionable canisters and those from the redundant newer canisters. In other words, the quality of the data from questionable gauges can be judged by the data recovered from the redundant gauges.

For example, reference to Figure 9 reveals that hole 7 was drilled on the 20-m ring on the same radial as hole 2 on the 10-m ring. But while canister 2-1 (Figure 11) appeared to experience questionable transverse-to-radial magnitudes, canister 7-1 (Figure 13) reveals a set of histories that is fully consistent with a shock environment dominated by radial motion (*i.e.*, large radial component accompanied by an insignificant transverse contribution). It is reasonable to expect that any test bed character such as joints that might cause the anomalous results at hole 2 would persist at hole 7. Since those anomalies are not persistent, canister rotation is a more likely explanation of the canister 2-1 response.

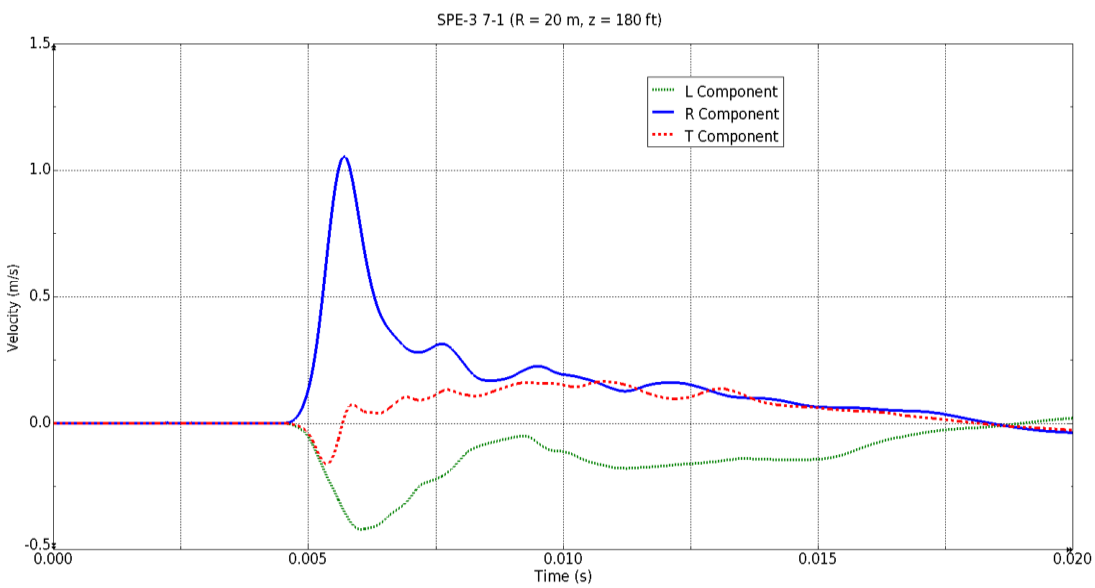

Figure 13: Velocity histories from location 7-1 for SPE-3.

Another example is the comparison in Figure 14 between data from older canister 3-2 and newer canister 8-2 which is nearby on the same radius ring (see Figure 9). The 3-2 canister transducers were inoperable for SPE-3 and so those data are from SPE-2; the data at 8-2 are from SPE-3. Other comparisons have already established consistency between those two events, and so comparison between these two sets of recordings is relevant. Specifically, Location 3-2 displays uncharacteristically high transverse negative amplitude accompanied by an insignificant radial record. But location 8-2 experienced a high outward radial velocity and a low-magnitude transverse velocity. As discussed in the prior example, it is unrealistic to conclude that the shock environment can change by such a large amount in the short distance between hole 3 and hole 8. It is more plausible to conclude that canister 3-2 rotated during installation.

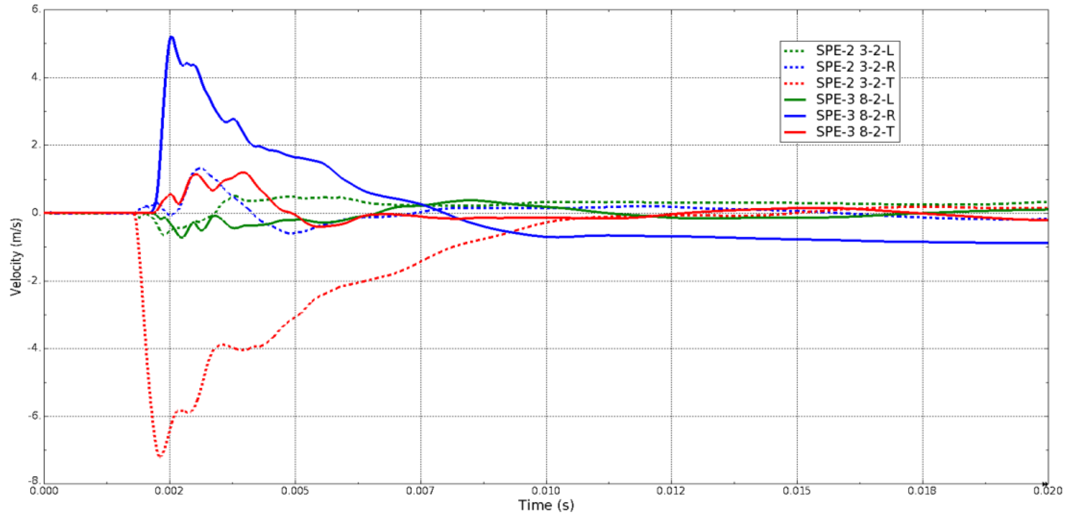

Figure 14: Velocity histories from location 3-2 for SPE-2 and location 8-2 for SPE-3.

Finally, reference to Figure 9 shows that older hole 6 is roughly in the middle of an arc between newer holes 7 and 9 on the 20-m ring. Canister 7-2 (Figure 15) and canister 9-2 (Figure 16) have reasonable relative radial and transverse motions while canister 6-2 (Figure 17) is unreasonable in this respect. Similar to other observations, it seems unlikely that the azimuth to hole 6 would have such a significant difference in the environment relative to the azimuths on either side.

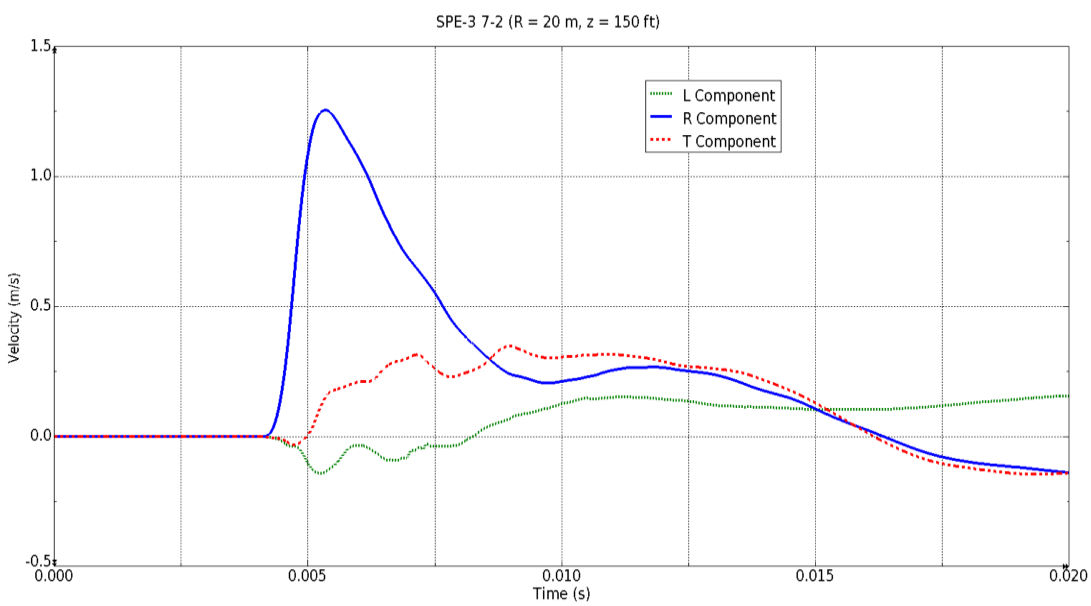

Figure 15: Velocity histories from location 7-2 for SPE-3.

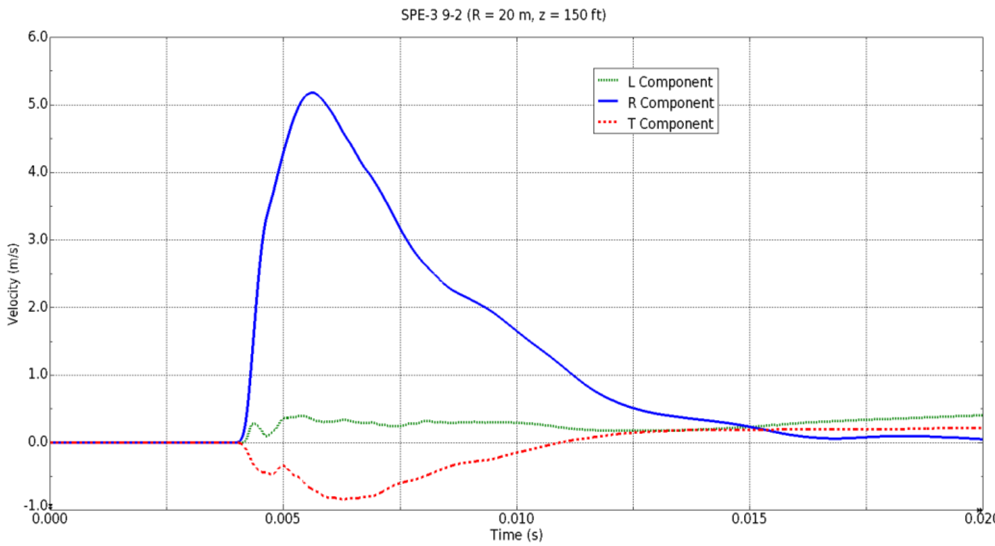

Figure 16: Velocity histories from location 9-2 for SPE-3.

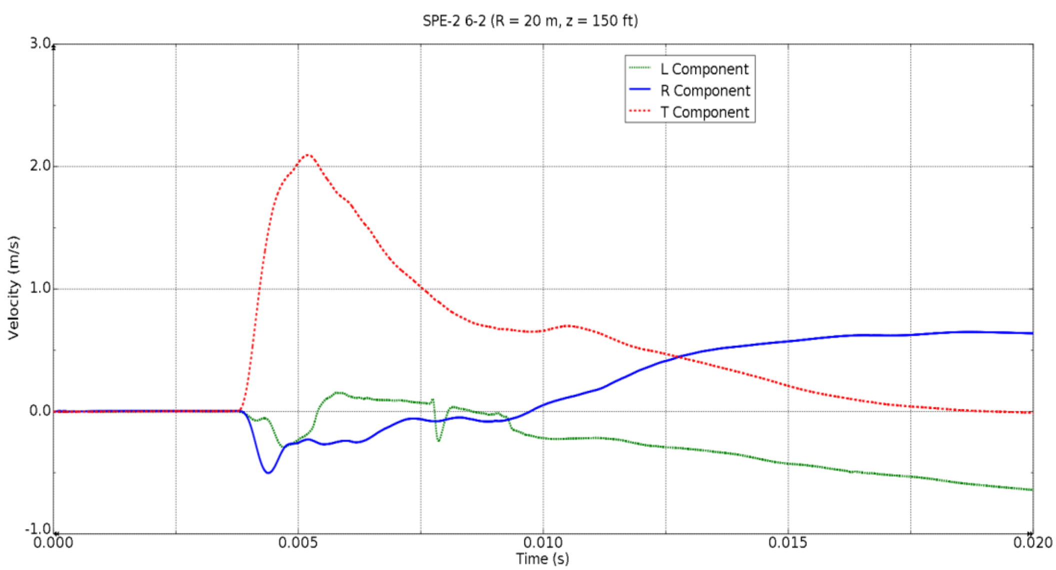

Figure 17: Velocity histories from location 6-2 for SPE-3.

The above discussion reviewed the relative horizontal components of canister histories. The general premise is that for a spherical or cylindrical explosive source the shock environment should be dominated by outward radial motion, with smaller contributions in the orthogonal tangential directions. Reference 5 presents more comparisons of these data that will not be repeated herein. Instead, the full SPE-3 data will be summarized by plotting in the radial peak velocity vs. the tangential peak velocity for every canister (Figure 18).

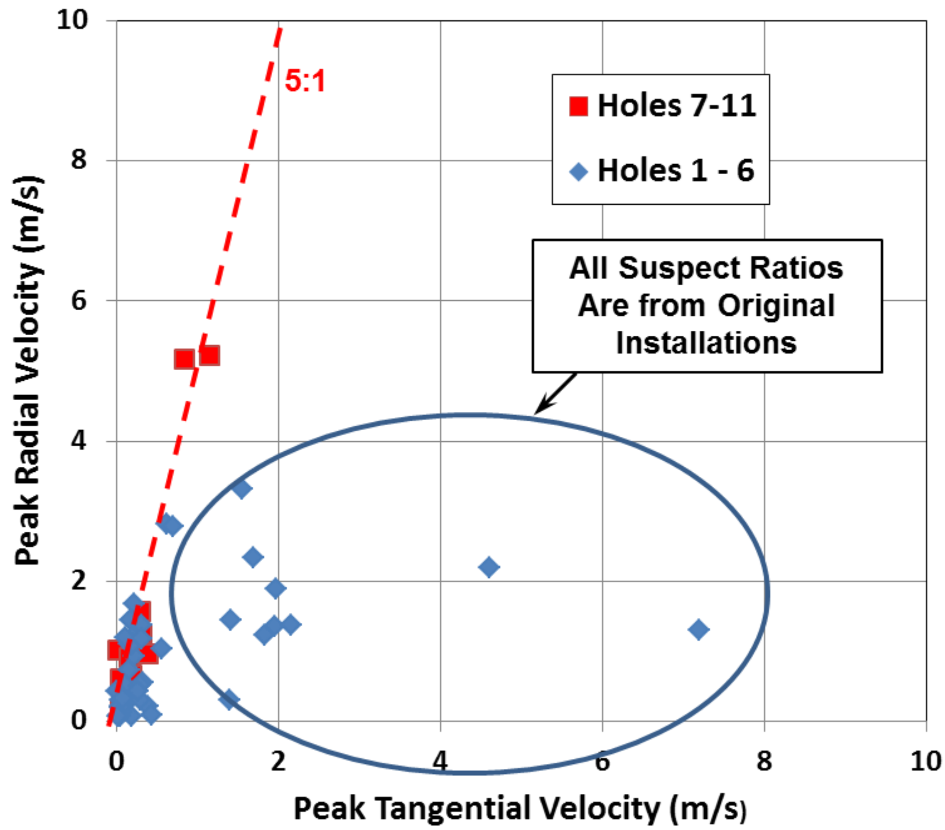

Figure 18: Peak radial velocity vs. peak transverse velocity for all canisters in SPE-3

A fit to the data from the newer holes suggests that the transverse velocity is about 20% of the radial velocity (*i.e.*, radial is five times the transverse). This is also true of a subset of the older canisters. However, a number of locations have peak transverse velocities that are equal to or greater than the respective peak radial velocity. All of those data points represent older installations. In other words, the response of all canisters installed using high quality control (holes 7 through 11) is clearly dominated by radial motion with no canister dominated by transverse motion.

A final summary of these data can be seen in Figure 19 which is an updated version of the "stop light" chart shown earlier. It repeats the chart from SPE-2 and includes a similar chart for SPE-3 including both the older and the newer canisters. The figure illustrates: 1) the older gauge response was consistent between the two events and 2) all new gauges provided reasonable data. Clearly, the questionable response in the older canisters is better explained by canister rotation rather than a hypothetical test bed phenomenology. These findings were presented in a briefing (Reference 5) to the SPE Subject Matter Experts (SME) panel and subsequently to the National Center for Nuclear Security (NCNS) Executive Advisory Board (EAB). The recommendation that the radial and transverse data from those gauges be corrected for rotations was accepted by both of these review groups.

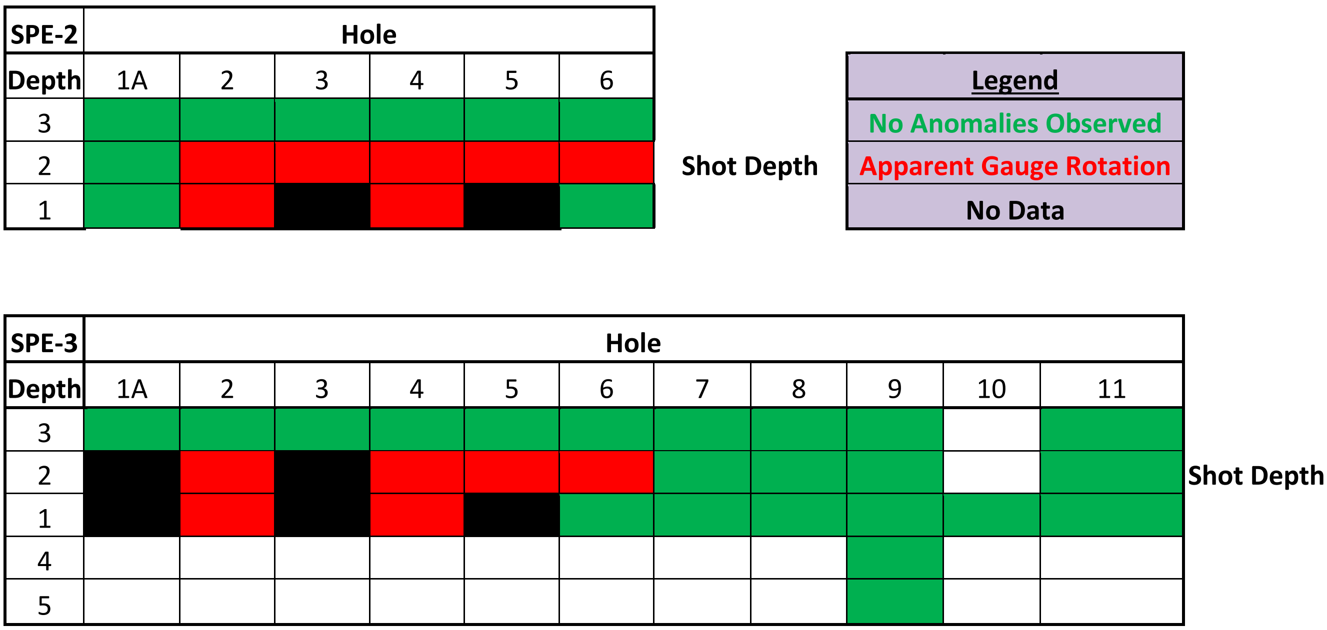

Figure 19: Figure 20: Stop light chart summarizing data for SPE-2 and SPE-3 including new gauge canisters.

DATA CORRECTIONS

Those corrections were performed as described in Reference 6. The details are available in that reference, and here we summarize that acceleration data were reviewed on a time step-by-time step basis. The radial and transverse records were resolved using trigonometric calculations, iterating on possible rotation angle, enabling the determination of the angle that provided the maximum outward radial motion for each location. The final reported radial and transverse records were altered to reflect this geometric correction.

TEST PHENOMENOLOGY

The availability of a corrected data set allows for confident study of test bed phenomenology. Specifically, peak velocity amplitude and velocity waveforms were studied to reveal details of the shock environment and rock response.

Shock Attenuation

A fundamental plot of ground shock data is peak velocity *vs.* yield-scaled range. But these pots must account for the fact that the drilled shot and the instrument holes, as a practical matter, are not straight vertical holes. These holes were surveyed after completion, and these data were used to determine the true range between the shot and any given canister. For example, Figure 21 illustrates the planned and actual location of the charge hole and the original seven instrument holes at the 150-ft depth. The data indicate that canister 2-2, which was planned to be at a range of 10 m, is actually only 8.35 m from the center of SPE-2. On the other hand, canister 1A-2, also planned for the 10-m range, is at 10.53 m. As the velocity attenuation rate is expected to be of the order -1.5 in log-log space, this is an important distinction.

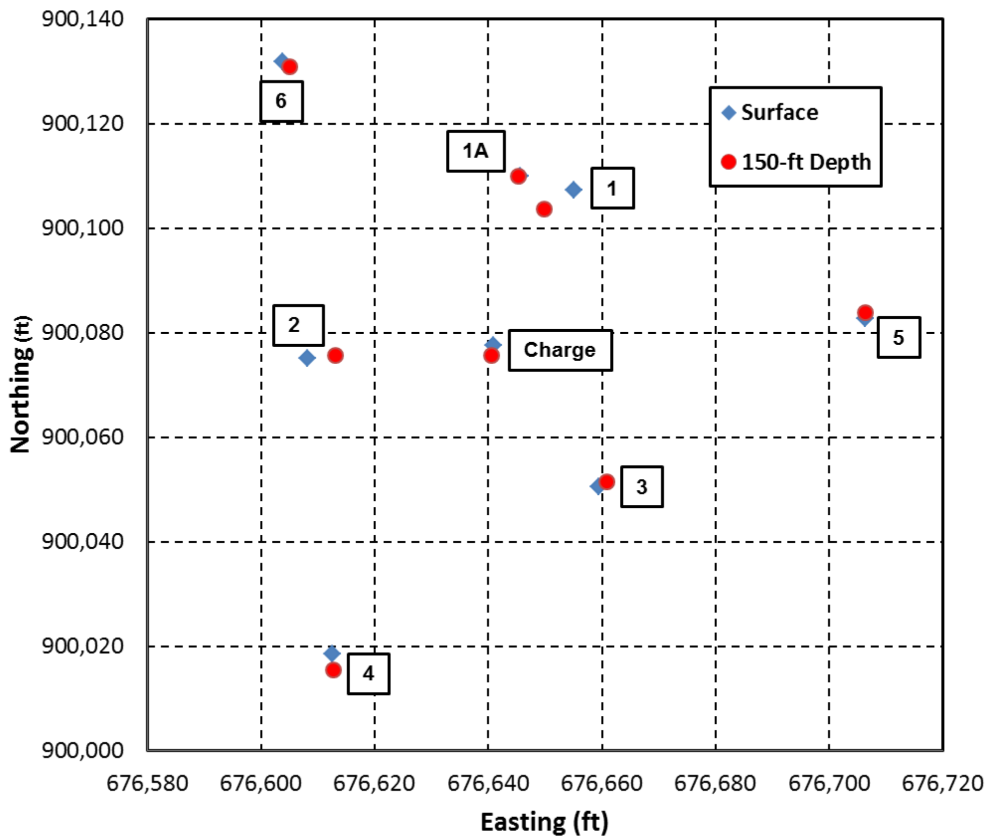

Figure 21: Test bed layout showing borehole locations at the surface and at 150-ft depth.

The peak radial velocities for the composite data set (*i.e.*, SPE-1, SPE-2, and SPE-3) vs. yield-scaled range are plotted in Figure 22. The data represent:

1) The peak of the record from the radial transducer as corrected by Thomsen (Reference 6) for canisters on the respective charge depth.
2) For canisters above or below the charge depth, but not at the 50-ft depth, the data represent the resolved value using the peak of the corrected radial measurement and the peak of the longitudinal measurement.
3) The peak of the record from the radial transducer, with no corrections required, for canisters at the 50-ft depth.

A regression fit to these data in log-log space is characterized by a correlation coefficient, r, of 0.92.

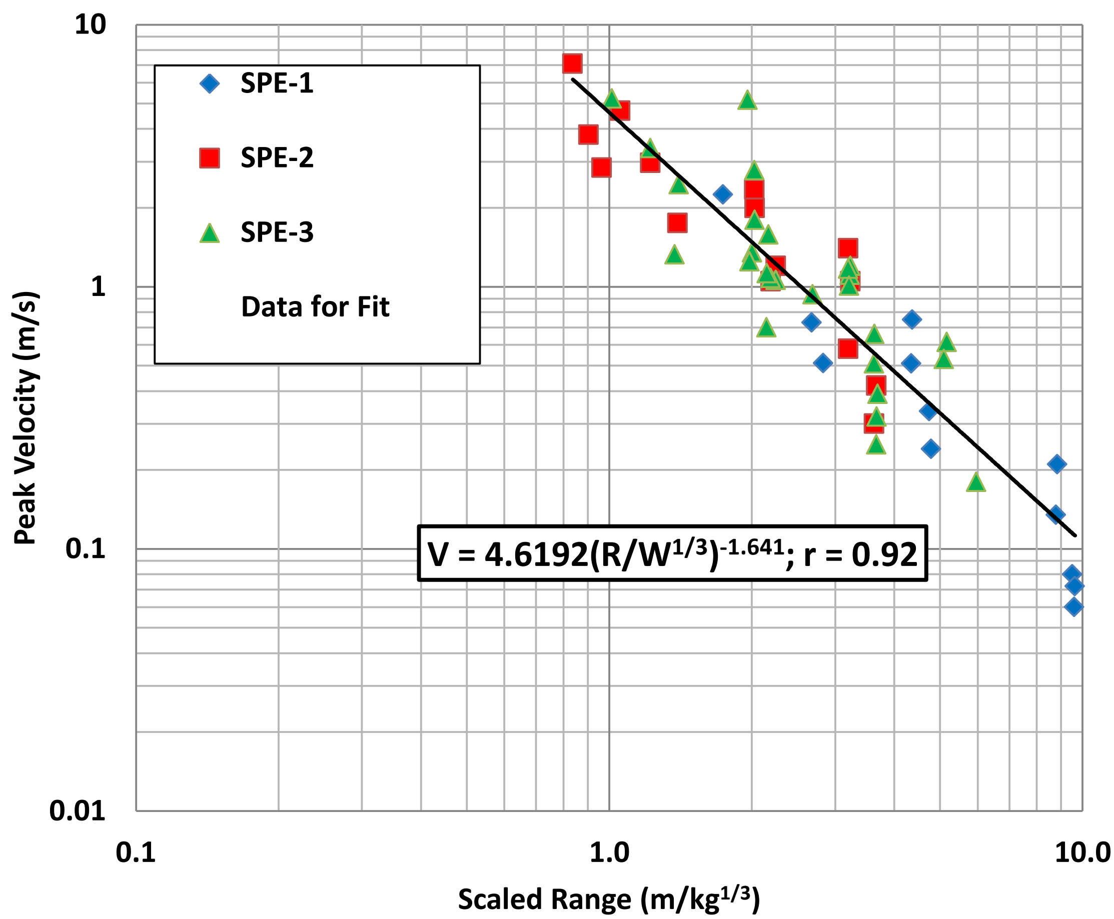

Figure 22: Peak radial velocity vs. yield-scaled range using corrected SPE-1, SPE-2 and SPE-3 measurements.

A similar plot was constructed using uncorrected data. The peaks of the uncorrected record for each radial transducer were used to construct Figure 23. As in Figure 22, longitudinal records were used where necessary to compute resolved radials for canisters not located at the charge depth. These data have a wider spread with a lower correlation coefficient of 0.78. In other words, the uncorrected data form a less consistent data set than the corrected data.

Shock Front Shape

SPE test bed drill cores revealed a highly jointed geologic setting including two major faults traversing the site. This raises concern over whether these characteristics will noticeably alter the ground shock emanating from the explosive sources of this test series.

To study this effect all of near field data were projected to a single plane through the shot for contouring. This is a standard analysis technique for viewing data on various azimuths at different locations. For a spherical or near-spherical shock environment the datum at any location can be projected from the spherical surface through that datum to any other location of the same radius from the source point. Taking all data to a common plane – say the horizontal plane through the explosive center – allows these data to be contoured in 2-D. Contours of the resulting data will result in circles concentric about the source. Conversely, for a non-spherical environment these data will not contour in a circular pattern.

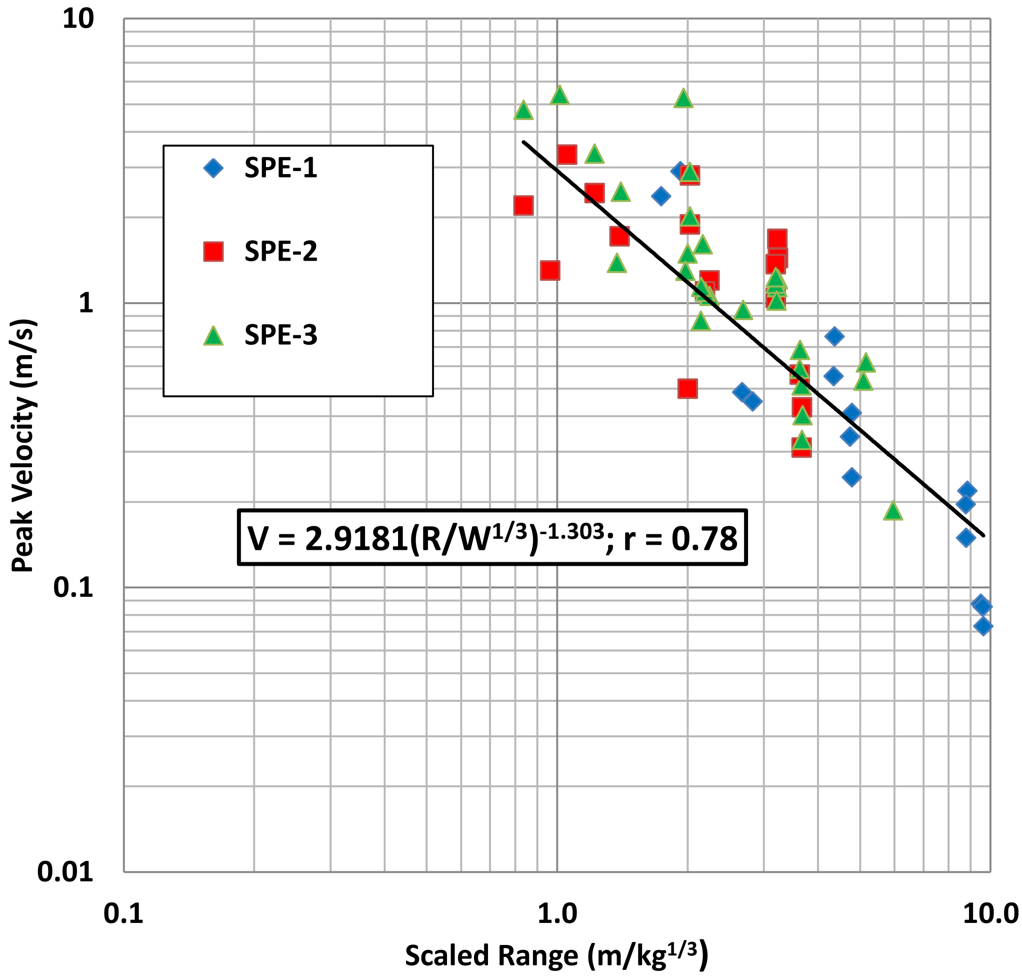

Figure 23: Peak radial velocity vs. yield-scaled range using uncorrected SPE-1, SPE-2 and SPE-3 measurements.

The corrected peak radial velocity data from SPE-3 were plotted in this manner in Figure 24. The contours are nearly circular about the source. The contours are actually offset from the source somewhat and centered on hole 3. This reflects the fact that there were no measurements taken within the actual charge. And while it is known that the largest amplitude velocity is necessarily at the source, the data are limited to locations no nearer the source than the 10-m ring canisters. Consequently, the contours are forced to center on the largest amplitude of the canisters in that 10-m ring.

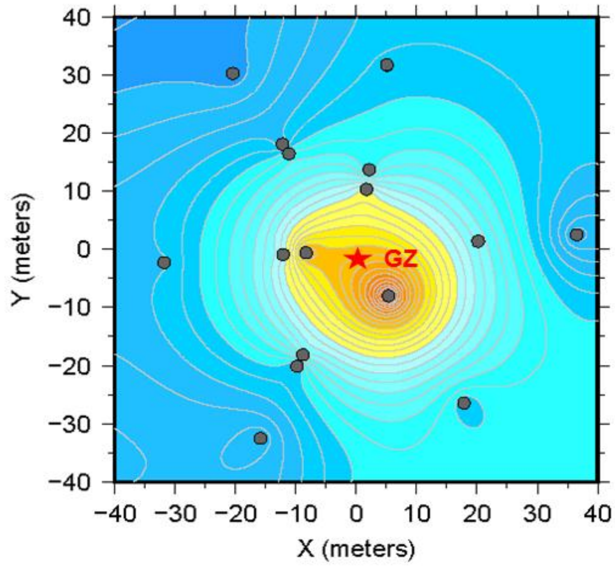

Figure 24: Contour plot of corrected peak radial velocity data for SPE-2 projected onto the shot plane.

By contrast, the same type of plot using uncorrected radial measurements is provided in Figure 25. The contours in this figure are more oval in character with a clear directionality of propagation inferred. These uncorrected data suggest a non-spherical shock front, and the analyst could easily be fooled that some local phenomenon in the test bed has an effect on the shock propagation, thus resulting in an erroneous model.

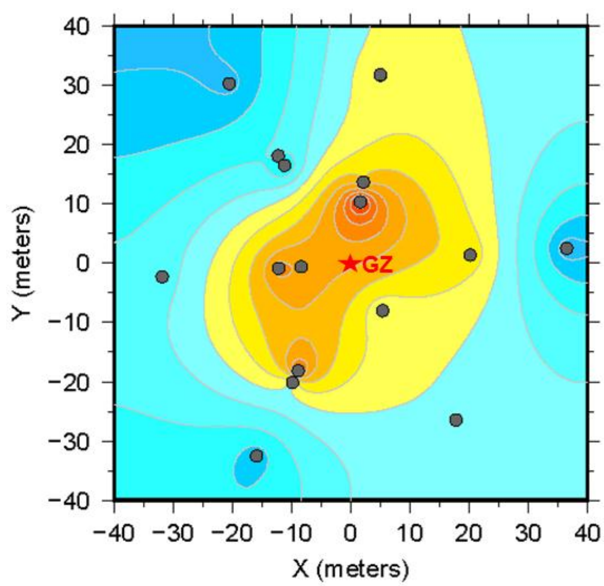

Figure 25: Contour plot of uncorrected peak radial velocity data for SPE-2 projected onto the shot plane.

Shear Waves

One of the primary objectives of the SPE series is to study shear wave content and to identify its source and phenomenology. Analysis of the corrected velocity waveforms helps to provide some insight from the perspective of the near field.

Figure 26 includes velocity waveforms from SPE-1 for the 10-m ring at the 150-ft depth. These canisters are approximately 45^o out and up from the source. As such, a pure compressional wave environment would produce longitudinal response identical in magnitude and character to outward horizontal response.

However, a review the data in this figure reveals other characteristics. For example, the radial (*i.e.*, outward horizontal) transducers are similar for both location 2-2 and 3-2 (upper plot and lower plot with peaks of 0.4 m/s and 0.42 m/s, respectively). And the rise portion of the longitudinal (*i.e.*, vertical) curves closely track the rise of the radial curves as expected. But both longitudinal waveforms are perturbed at about the time of the peak of the radial history. The longitudinal for 2-2 inflects upward dramatically and achieves significantly (about 50%) greater amplitude than the radial. Location 3-2 shows a coincident arrival on its longitudinal record as highlighted by the vertical dashed line. The peak for this record is “clipped,” or lower than the radial. Though this suggests different phasing than occurred at 2-2, it is still clearly a second wave arrival with the same wavespeed as the second arrival at 2-2. Moreover, the oscillatory nature of the both longitudinal waveforms provides a strong suggestion that these transducers are responding to a strong shear wave superimposed upon the compression waveform.

Another manifestation of shear waves is evident in both the radial and transverse measurements at location 9-1 in SPE-3 (Figure 27). This location (180-ft deep on the 20-m ring) for this event is 26^o below the charge. As expected for an angle between 0^o and 45^o there is significant longitudinal (downward vertical) response although of lower amplitude than the radial (outward horizontal). But there are other characteristics of interest. The initial transverse velocity is very low in magnitude relative to both of the other measurements. However, there is a distinct arrival pushing its amplitude up to near the levels of the longitudinal measurement as denoted by the vertical dashed line. Moreover, the radial waveform has a “double-peak,“ and the transverse waveform takes on an oscillatory nature. There also is alignment between oscillations in the transverse and the longitudinal waveforms. These aspects likely result from shear waves superimposed on the compressional shock.

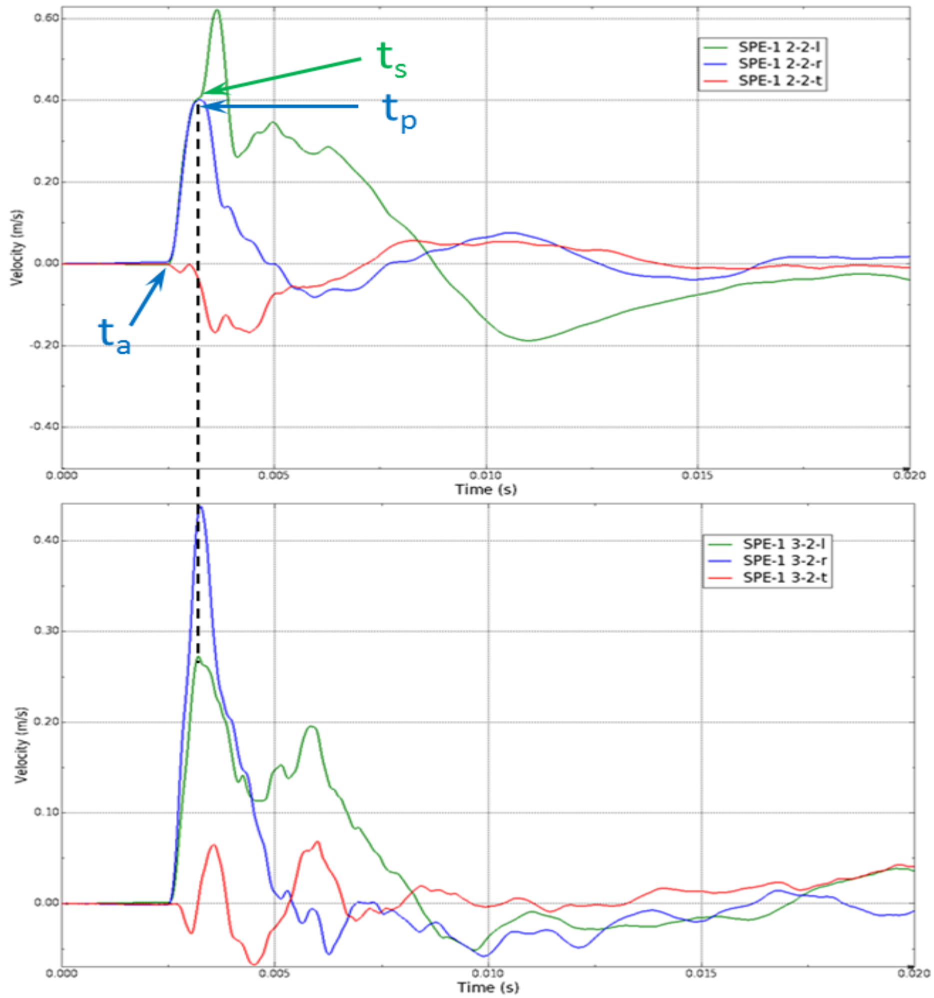

Figure 26: Corrected SPE-1 velocity waveforms for location 2-2 and 3-2.

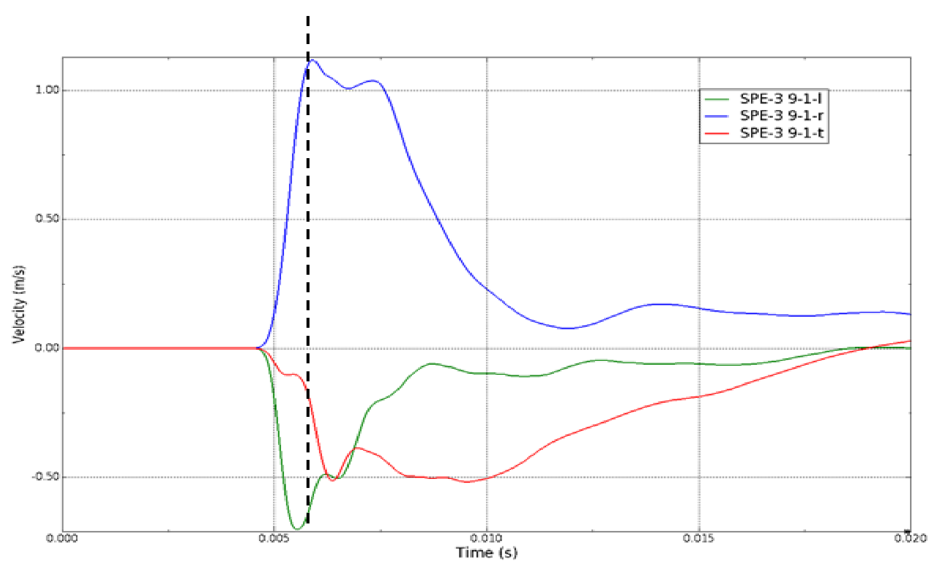

Figure 27: SPE-3 velocity waveforms for location 9-1.

Similar evidence of shear phenomenon is seen throughout the data set for the three events. A summary of shear wave arrival times for SPE-1 is illustrated in Figure 28. Three notable characteristics are observed. These observations and their relevance are summarized below.

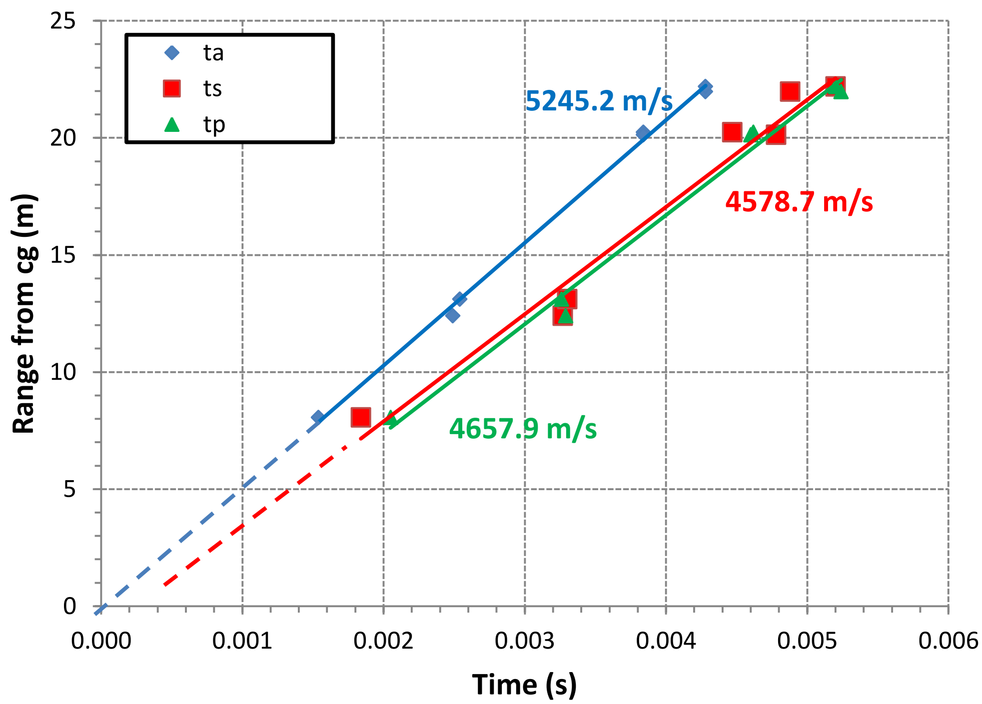

Figure 28: SPE-1 near field accelerometer arrival times; first arrival, peak arrival and shear arrival.

First, the shear wavespeed is slower than the compression wavespeed, which is signified by the first arrival. This is expected based on simple mechanical relationships between compression and shear.

Second, the shear arrivals are somewhat coincident with the arrivals of the peaks. This implies that the shears waves might either clip or amplify peak radial magnitude, thus exacerbating the data spread. That is, without the late-arriving shear, the radial velocity data might have an even tighter spread than that defined in Figure 22.

Finally, the fit to the shear arrivals trends toward the origin of the plot. This implies that the shear waves originate at the explosive source. Specifically, since (0, 0) on this plot represents is the detonation time and detonation point of the explosive, the shear arrivals trending to (0, 0) implies the explosive as the source of the shear waves. A postulated source of the shear content is the local test bed jointing described earlier. For the alternative explanation that distributed joint sets cause the shear, the source would thus be distributed, and the plot of shear arrival times vs. range from the explosive would be a random, uncorrelated set.

Figure 29 and Figure 30 are similar plots for SPE-2 and SPE-3, respectively. The same trends are observed. That is, in each case the shear wavespeed and peak wavespeed are similar and they are, as expected, lower than the compressional wavespeed. Further, the trend of the fit line to the shear arrivals in each these cases also points to the detonation point and time. These plots provide consistent evidence that the explosive charge is the source of shear waves.

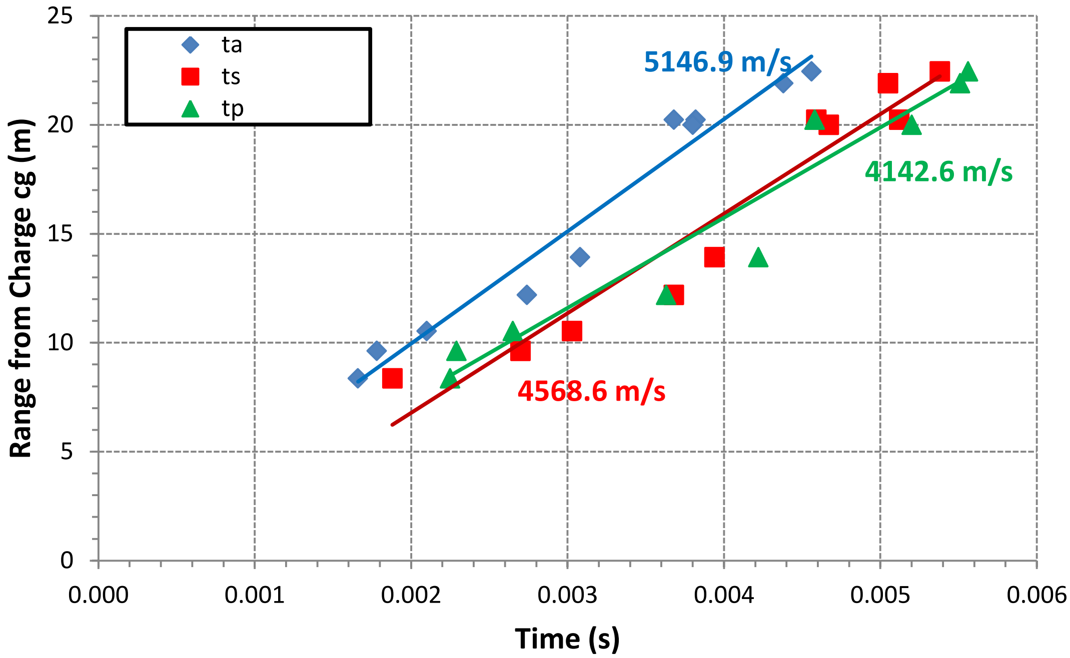

Figure 29: SPE-2 near field accelerometer arrival times; first arrival, peak arrival and shear arrival.

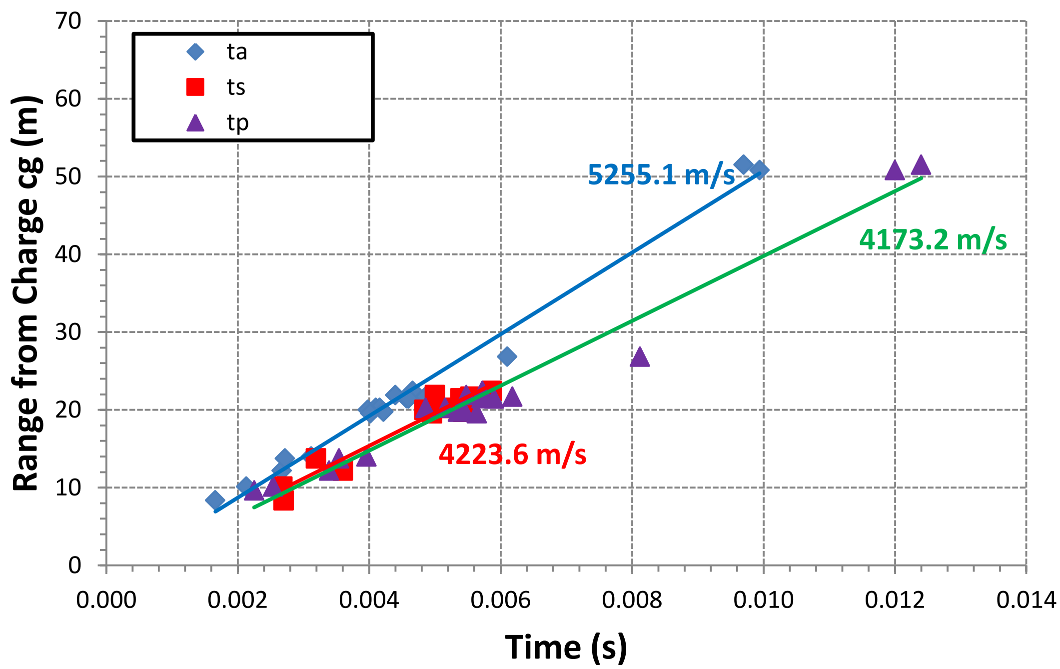

Figure 30: SPE-3 near field accelerometer arrival times; first arrival, peak arrival and shear arrival.

These shear waves and identification of their source are a critical component of this program. Ideally, the program considers spherical sources and analysis is aimed at determining phenomenology that will generate this energy. But for reasons practical to construction (*e.g.*, container fabrication, drill hole diameter, *etc*.) cylindrical sources – such as those emplaced for SPE – are used a proxy for the equivalent sphere. However, since the waveform analysis suggests that the cylindrical charge shape could be a major source of shear waves in these experiments, a cylinder may not be a proper proxy for a spherical source. This assessment is bolstered by reviewing Figure 31 which illustrates the theoretical radiation pattern for a cylindrical source. The figure demonstrates that considerable shear content should be expected from this shape. In contrast, the theoretical radiation pattern from a spherical source is purely compressional. So assumption that a cylinder is an acceptable proxy for a sphere, or that we can neglect the source shape when trying to understand shear content, should be re-visited.

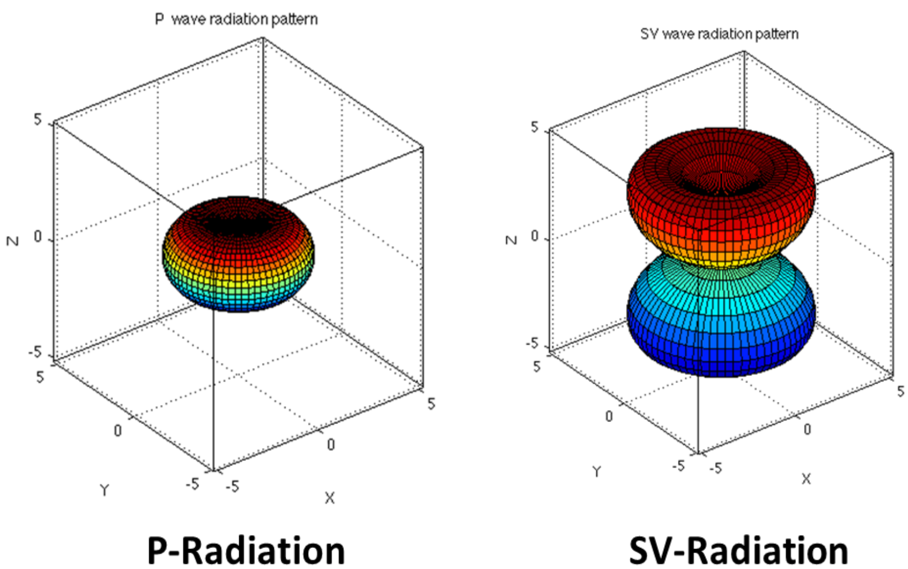

Figure 31: Theoretical radiation patterns form a cylindrical source

Site Damage

As discussed above, comparisons between SPE-2 and SPE-3 data confirmed that several of the instrument packages installed prior to the SPE-1 and SPE-2 events rotated during installation. We noted that velocity histories at the same or redundant locations were similar in character. But there were some differences in the data from the two events that only received passing notice in that discussion. Specifically, we noted an instance where the SPE-3 histories were lower in amplitude and had later arrivals than those from SPE-2. Figure 32 and Figure 33 are two examples of this.

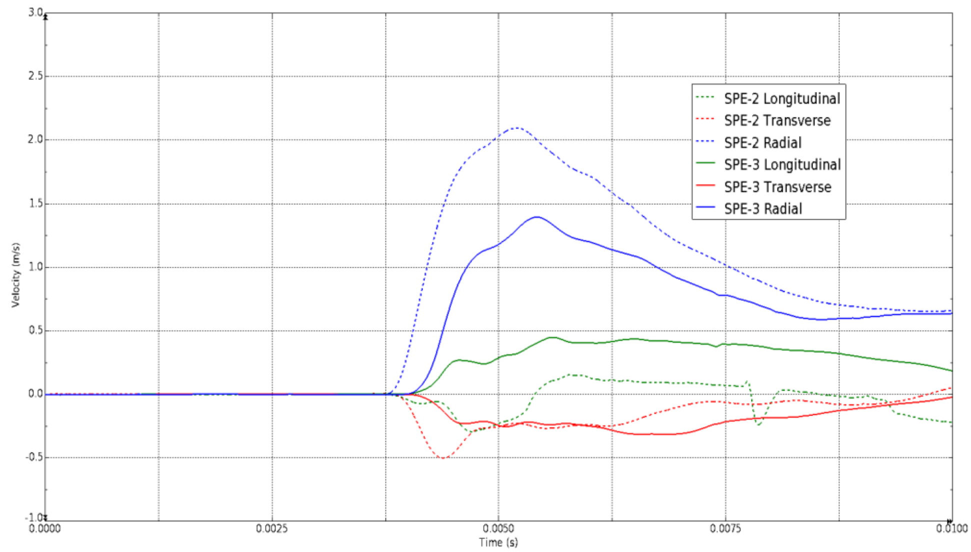

Figure 32: Velocity histories from corrected accelerometer data recorded by canister 6-2 in SPE-2 and SPE-3.

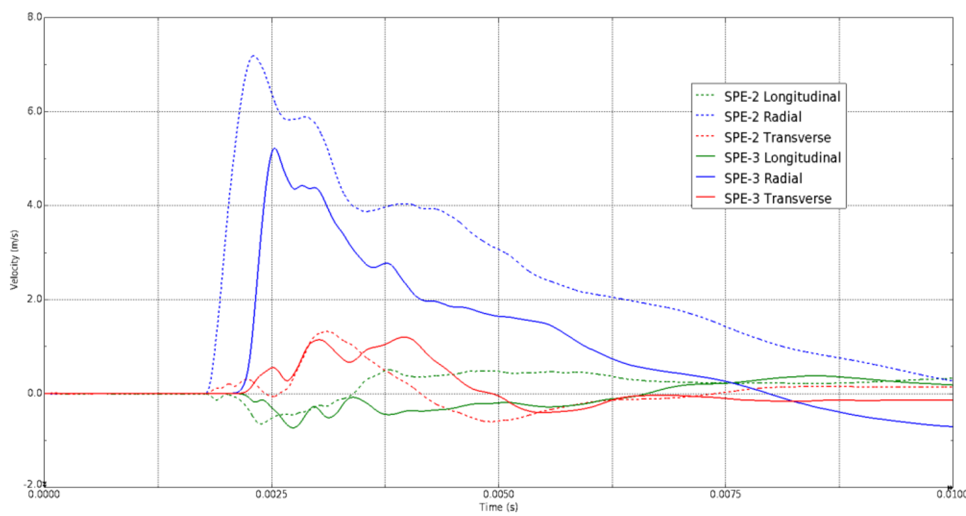

Figure 33: Velocity histories from accelerometer data recorded by canister 3-2 in SPE-2 and by canister 8-2 in SPE-3; histories for 3-2 have been corrected for rotation.

The data in Figure 32 are from canister 6-2, corrected for approximately 90^{o} rotation. The corrected radial history for SPE-2 (dashed blue line) is significantly higher in amplitude and has a much earlier arrival despite the otherwise similar character to the corrected radial history for SPE-3 (solid blue line).

The data in Figure 33 are from canister 3-2 in SPE-2 (dashed lines) and from redundant canister 8-2 in SPE-3 (solid lines). These data were presented earlier as well (Figure 14) for a case where an originally installed canister (3-2) appeared to have rotated 270^{o} (that is, a transverse measurement that appears to be a radial motion except for its inward – *i.e.*, negative – direction). Its redundant replacement (8-2) is quite similar in character and the radial measurement has the correct motion relative to its other components. But like location 6-2 the SPE-3 data are lower in amplitude and have a later arrival.

Similar comparisons are provided in Reference 9. A summary of the general observations is illustrated in Figure 34. This figure contains a plot of time of first arrivals vs. range for all near field measurements in both SPE-2 and SPE-3. The dashed line fits to the separate test data sets are included and illustrate that the SPE-3 propagation speed is slower (has a lower slope fit) than that for SPE-2.

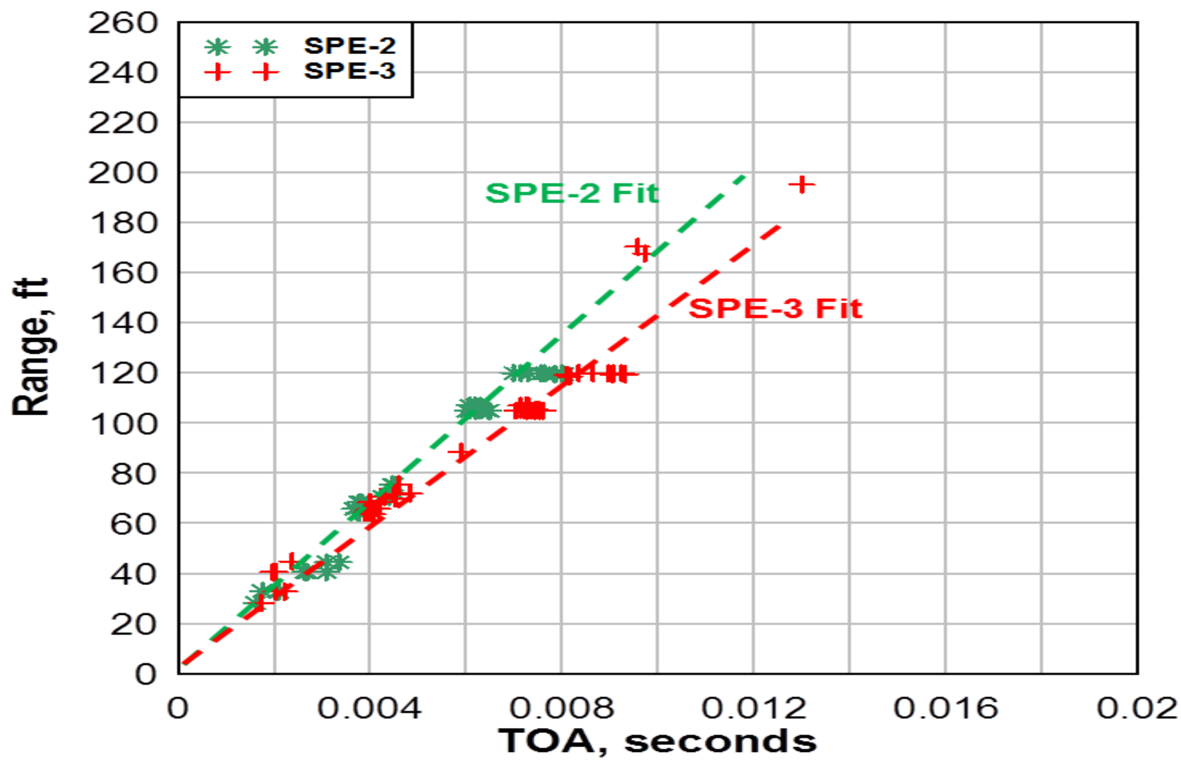

Figure 34: Time of first arrival vs. range for SPE-2 and SPE-3. (from Ref. 10)

In an alternative presentation of these data the *difference* in the arrival times for canisters fielded in both SPE-2 and SPE-3 is plotted against range in Figure 35. This plot includes data from the near-source surface accelerometers as well, the layout for which is included as Figure 36. Note that the symbols on Figure 35 refer to the symbols on Figure 36. That is, the purple triangles represent surface accelerometers on a 15-m ring surrounding the shot hole while the green squares represent surface accelerometers 30 m or more distant from the shot hole. This includes both those gauges in a 30-m ring surrounding the hole as well those in a in linear array extending out to the 90- range m in 15-m increments. The blue diamonds represent the buried near field gauges discussed throughout this report.

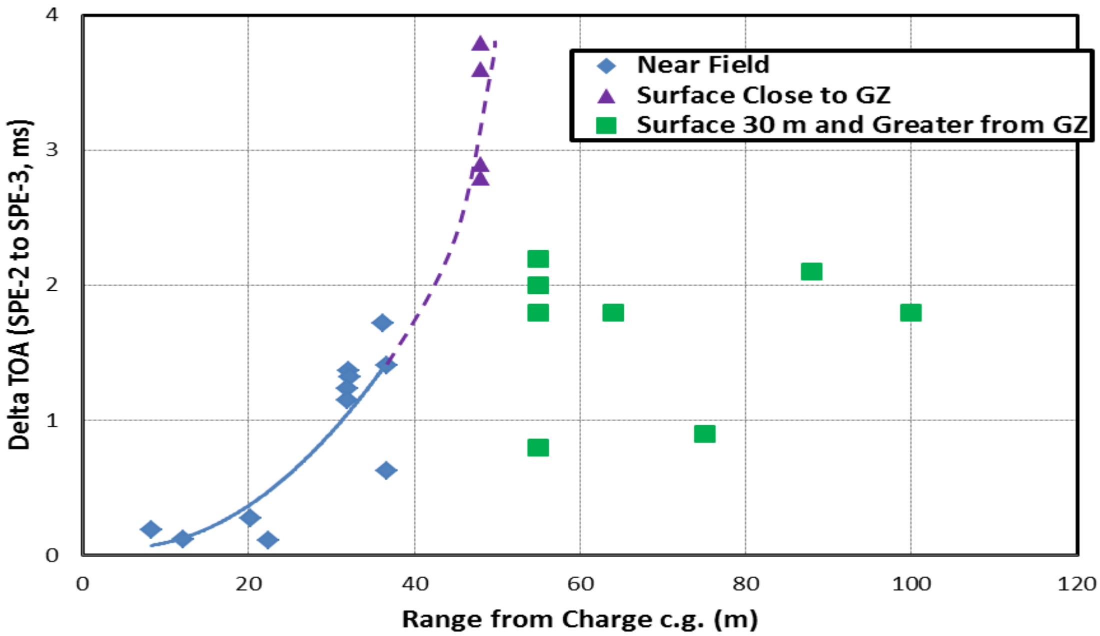

Figure 35: Change in first arrival time between SPE-2 and SPE-3 vs. range.

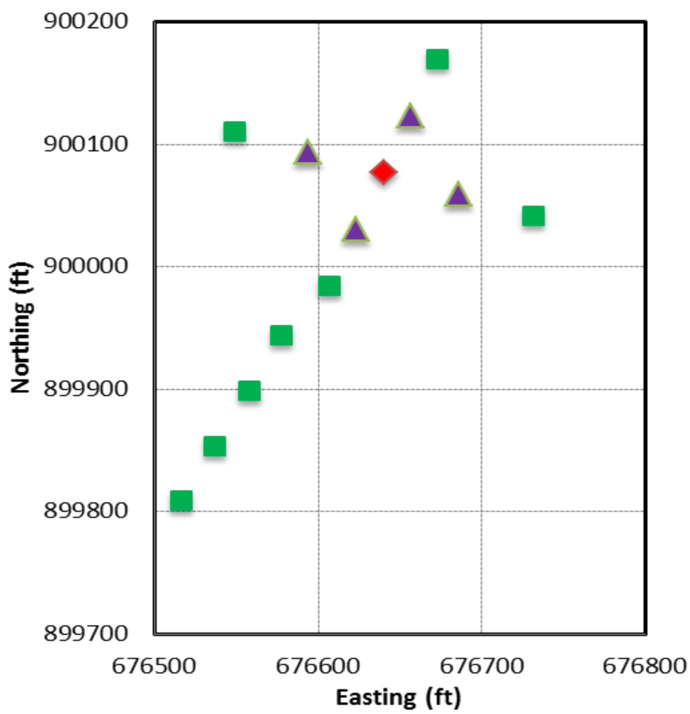

Figure 36: SPE-2 and SPE-3 surface accelerometer array.

There is a distinct trend of increasing difference in arrival time with distance from the source for the near field gauges and the close-in surface accelerometers. On the other hand, those surface accelerometers that are more distant from the shot hole have a more or less constant delay of 2 ms except for two outlier gauges. This can be interpreted as the waves traversing a cone of damage above the shot that was caused by SPE-2 similar to the conceptual representation shown in Figure 37. Shock travelling through this damaged zone will travel at a reduced speed. And while waves travelling exclusively within this damaged zone will continue to accumulate delay relative to the SPE-2 waves, once a wave leaves this zone (*i.e.*, leaves the cone of damage) the delay will be fixed as the wavespeed reverts to the un-damaged value.

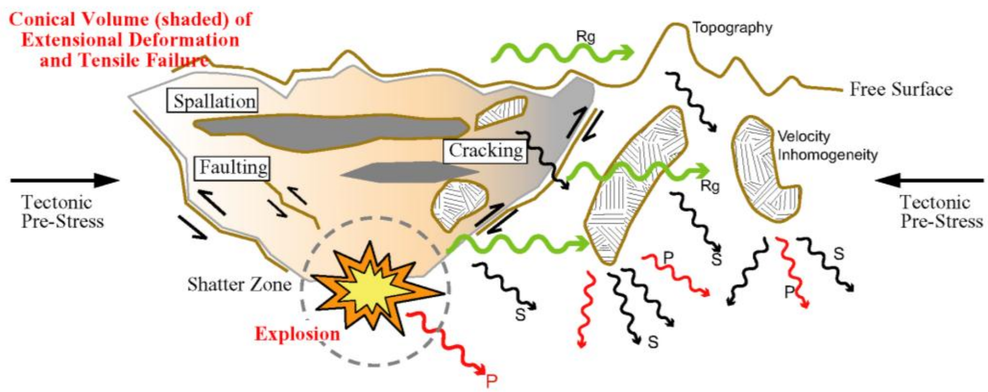

Figure 37: Hypothetical damage phenomenology from a buried source.

Figure 38 is a plot peak radial velocity from SPE-2 compared to the same value for SPE-3 for canisters fielded in both events. The 1:1 line representing equality between values is also shown. Most data points are below the 1:1 line implying that SPE-3 amplitudes are consistently less than SPE-2 values. As these events were nominally identical, this must be explained due to SPE-3 shock travelling through weakened rock.

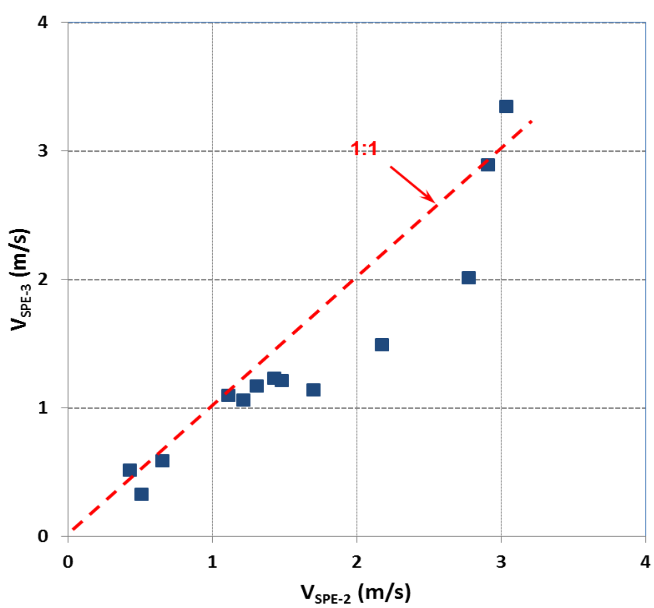

Figure 38: Comparison of peak radial velocity for SPE-2 and for SPE-3.

These plots (Figure 34, Figure 35, and Figure 38) use data from active measurement systems to present evidence of damage caused by SPE-2. The evidence includes an extent of damage – or a damage cone – extending above the shot and out to some range. Figure 39 is a plot of cracks mapped on the surface of the SPE site after completion of SPE-3. The extent of cracking is consistent with the observation from Figure 35 regarding the damage extent implied from surface accelerometer arrival times.

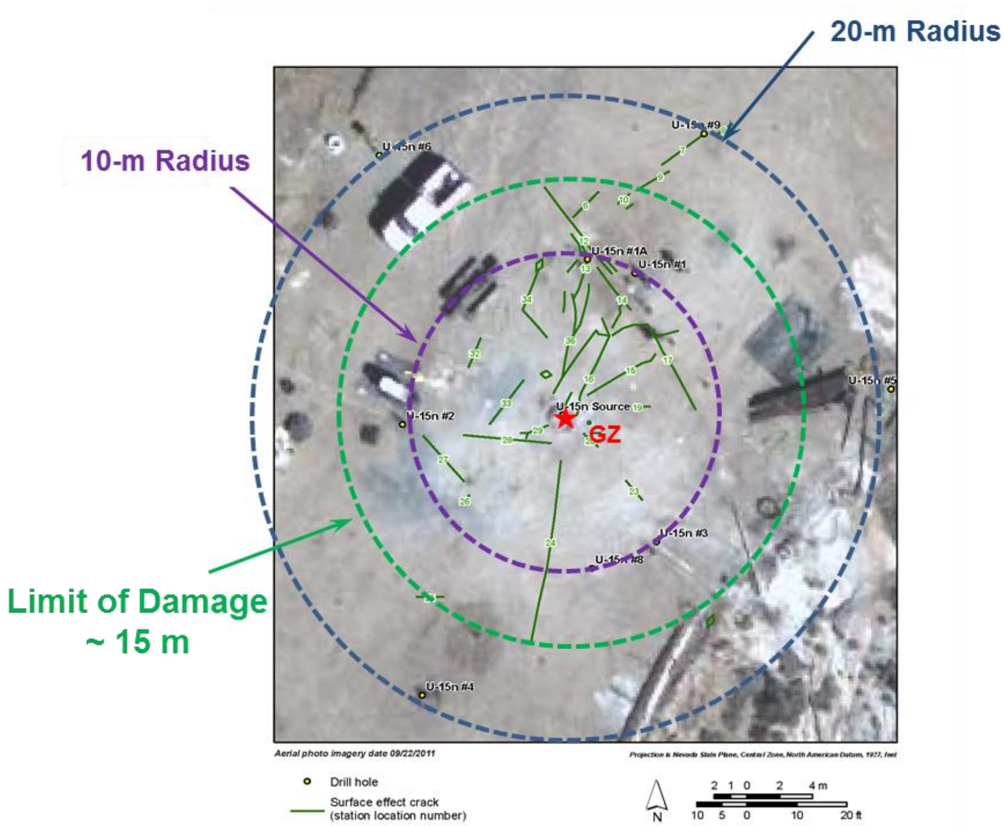

Figure 39: Surface cracks identified at the SPE test bed after SPE-3. (Ref. 11)

Subsurface Topography

The bulk of this report considers the data recorded by the buried near field accelerometer array. Here we continue analysis of the surface accelerometers to study subsurface geologic features. This set of gauges includes A6, A7, A10, and A11 on the 15-m ring and A5, A8, A9, and A12 on the 30-m ring, and tis analysis uses arrival times and slant ranges for these gauges to compute apparent velocity.

Figure 40 includes the velocity histories for A5, A6, A7, A10, A11, and A12. A study of this plot reveals some unexpected behavior. Although A6, A7, A10, and A11 are equidistant from the source they form two distinct sets for arrival time: arrivals at A7 and A10 are nearly coincidental; arrivals at A6 and A11 are nearly coincidental, and later than arrivals at the A7/A10 pair. Also, while the arrival at one 30-m range gauge (A5) is later than all 15-m range gauges as expected, the arrival for A12, also at the 30-m range, is earlier than two of the 15-m range gauges just discussed (*i.e.*, A6 and A11).

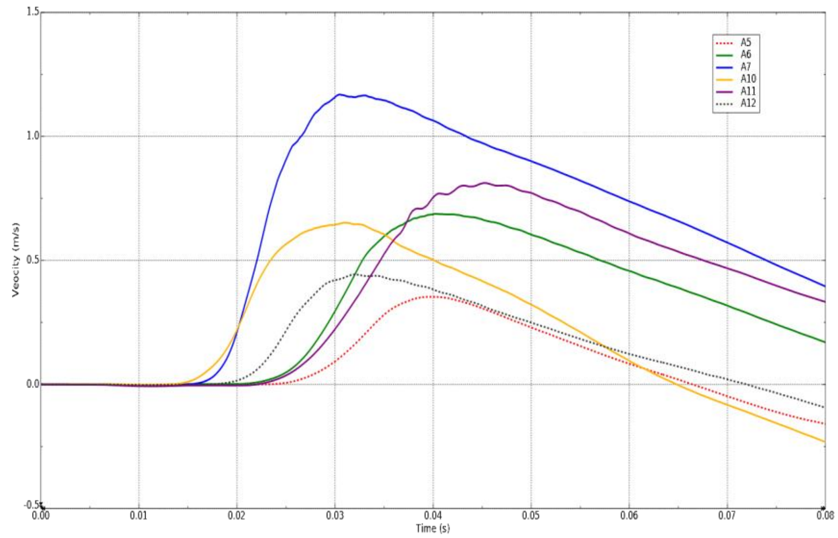

Figure 40: Velocity histories from the 15-m ring and 30-m ring surface accelerometers.

This is suspicious behavior but further insight is gained by computing apparent velocities for each surface accelerometer and developing contours of these values using the spatial layout of these gauges within the test bed (Figure 41). These contours indicate a clear trend to the southeast. Analysis of the drill cores described earlier revealed an upper weathered layer overlying the intact granite of the site. If we assume that each layer exhibits a constant velocity these data suggest a southeast dipping interface between the weathered and the intact granite. This is supported by the seismic reflection data illustrated in Figure 42.

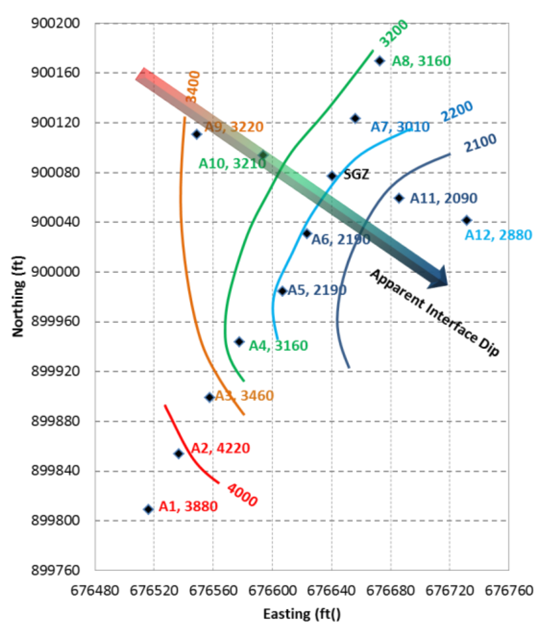

Figure 41: SPE-2 surface accelerometer array, including computed apparent velocity values and contours.

Revisiting the anomalous A12 value, we note that this gauge was placed on the shoulder of the access road leading up to the test bed rather than on the test bed. Consequently, this gauge is several meters lower in elevation than the remaining surface accelerometers which are on the test bed. This would create a shorter travel distance from the source, resulting in a faster apparent velocity.

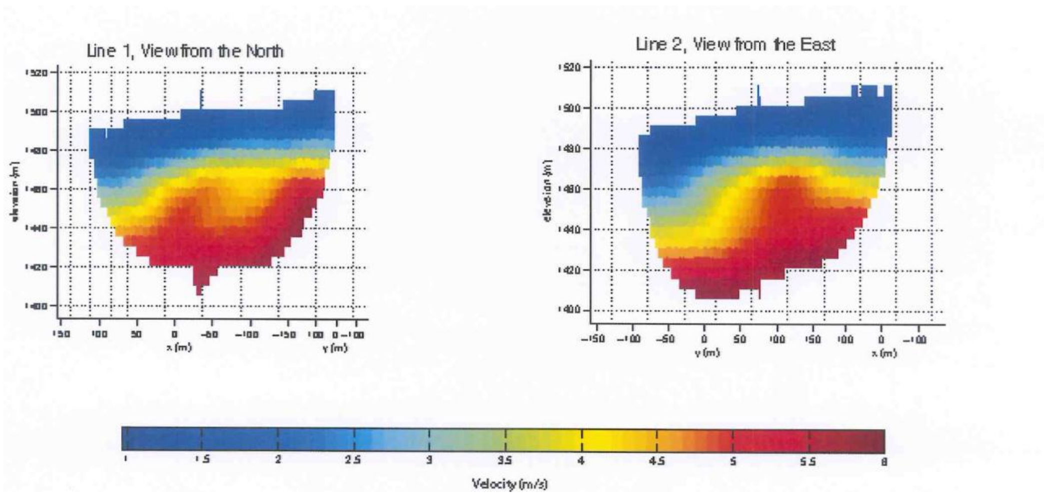

Figure 42: Wavespeed contours from seismic reflection survey of the SPE test site. (Ref. 12)

SUMMARY AND RECOMMENDATIONS

Summary

This report demonstrated that a number of the gauge packages active for SPE-1 and SPE-2 rotated during placement. Plots of uncorrected data (*i.e.*, assuming that labeled components were pointed in the desired direction) are inconsistent with the shock environment expected from an explosive source. Further, the data histories exhibit considerable inconsistency between measurement locations and the peak amplitudes of these data exhibit significant scatter.

Based on these observations new instrument packages were installed prior to SPE-3. All of the data from this new set of gauges were consistent with expectations for an explosive source. Individual gauges active in all three tests provided consistent results from test to test. And the new installations which were redundant to these older installations provided a clear contrast in SPE-3 data to the older gauges. We conclude that some number of the older installations rotated during installation.

The degree of rotation for each canister was estimated, and the data for gauges were corrected to reflect this. The resulting set of histories provides a self-consistent data set and the peak amplitudes demonstrated considerably less scatter.

The corrected data set permits a credible analysis of near field phenomenology of the first three SPE events. This analysis reveals the following:

- The shock front from these events is consistent with a spherically propagating pulse.
- Significant shear wave content is discernible from the set of records and the late time, post front environment may not be spherical in nature. The shear content appears to emanate from the explosive source. There is no evidence in the data to support whether either the faults or the joint sets at the test site are the source of any noticeable shear waves.
- The data suggest that SPE-2 caused damage to the near source region which affected the shock environment caused by the SPE-3 detonation.
- The surface accelerometer data suggest a sloping interface between the weathered zone and the intact granite which should be considered in developing models of the test site.

Recommendations

The following recommendations are derived from the analysis of this report:

1) Data from canisters installed prior to SPE-3 should be corrected for rotations in the manner performed by Thomsen (Ref. 6). These corrected data should be considered the validated data set for SPE-1, SPE-2, SPE-3 and any subsequent SPE events at this location.
2) The SPE test series should include a spherical emplacement designed to allow for comparison between environments created by spherical vs. cylindrical charge geometry. We consider the detailed repeatability of data between events SPE-2 and SPE-3 at the same location and with nominally the same yield. One might reasonably assume that similar repeatability might be achieved at the SPE-1 location. However, while a new event at this location event would repeat the SPE-1 yield, we recommend substituting a spherical charge. If the resulting data are similar to the SPE-1 data then the cylinder can be considered to be a reasonable proxy for the sphere. Conversely, if the data between these two tests are significantly different (*e.g.*, less shear content from the spherical source) this would argue that a cylinder is not a reasonable proxy for a sphere when considering ground shock generated by an explosive charge.
3) Additional instrumentation would be helpful for better identifying the spall and damage zone for the SPE site. An array of vertical accelerometers within the suspected spall depth and near to the source hole would be helpful in this respect.
4) Additional post-event coring will also be helpful in delineating damage extent and laboratory tests of cores would help to define how the damage is manifest in rock properties. This coring and subsequent tests is also recommended.

References

1. Antoun, T., *et al*, "Analysis and Simulation of Near-Field Wave Motion Data from the Source Physics Experiment Explosions," 2011 Monitoring Research Review 2011, Lawrence Livermore National Laboratory, 2011.
2. Steedman, D. W., "LANL Review of SPE-2 Near Field Velocity Data," Presented to the SPE SME Data Review, Los Alamos National Laboratory, Los Alamos, NM, January 2012.

3. Steedman, D. W., “Supplement to: LANL Review of SPE-2 Near Field Velocity Data,” Presented to SPE Data Review Team, Los Alamos National Laboratory, Los Alamos, NM, January 2012.
4. Shah, K., personal communication, 2011
5. Steedman, D. W., Shah, K., and Hemming, X., “Review of SPE Near Field Accelerometer Data,” Presented to the NCNS Executive Advisory Board, 13 September 2012
6. Thomsen, J., “SPE Data Acceleration Component Rotation Methodology,” Applied Research Associates, Albuquerque, NM, 22 October 2012.
7. Townsend, Margaret, Prothro, L.B., and Obi, C., “Geology of the Source Physics Experiment Site, Climax Stock, Nevada National Security Site,” DOE/NV/25946—1448, National Security Technologies, LLC, Las Vegas, Nevada, March 2012
8. Brunish, W., et al, “Source Physics Experiment-2 Free Field Predictions,” Los Alamos National Laboratory, Los Alamos National Laboratory, Los Alamos, NM, 2011.
9. Steedman, D., “SPE-2/SPE-3 Near Field Data Review and Implications MRR 2012,” presented at the Source Physics Experiments Workshop, Monitoring Research Review 2012, Albuquerque, NM, 20 September 2012.
10. Thomsen, J., “SPE Accelerometer Data Analysis: Preliminary Results,” presented to SPE SME Group, Las Vegas, NV, 29 August 2012.
11. Drellack, S., et al, “Geologic Surface Effects Mapped Following Source Physics Experiment 3,” National Security Technologies, LLC, August 21, 2012.
12. Abbott, R., personal communication, Sandia National Laboratories, Albuquerque, NM, 2012.